Aalto University
School of Engineering

Lauri Kuuliala

Feasibility study of a semi-empirical simulation model for level ice breaking

School of Engineering

Thesis submitted for examination for the degree of Master of Science in Technology.
Espoo 12.1.2015

Thesis supervisor:

Professor Pentti Kujala

Thesis advisor:

Floris Goerlandt, M.Sc.

AALTO UNIVERSITY
SCHOOL OF ENGINEERING

ABSTRACT OF THE
MASTER'S THESIS

Author: Lauri Kuuliala

Title: Feasibility study of a semi-empirical simulation model for level ice breaking

Date: 12.1.2015 Language: English Number of pages: 7+58

Department: Department of Applied Mechanics

Professorship: Marine Technology Code: Kul-24

Supervisor: Professor Pentti Kujala

Advisor: Floris Goerlandt, M.Sc.

A semi-empirical method, presented by Biao Su, for simulating the motions and ice loads of a ship in the continuous mode of ice breaking, was implemented with some changes. The feasibility of the method was investigated by a sensitivity study of the empirical parameters of the model and the results were compared to other methods and full-scale data.

The simulation method uses a model for level-ice breaking, that assumes the breaking pattern of ice to be dependent on the relative motion of ice and the ship. Ice is assumed to fail by bending in circular sectors from the parent ice sheet. The forces acting on single hull-ice contacts are calculated and the global loads affecting the motions of the ship are resolved as well as local loads.

The simulation method can be used to determine maximum speed, ice resistance and ice loads in given ice conditions. The results were found to be sensitive to the empirical parameters of the model. Some parameter combinations also led to erratic behavior of the model.

Overall, the predicted speeds, resistances and ice loads were within reasonable limits. However, there was significant scatter in the results arising from the choice of the values of the empirical parameters.

Keywords: Ice breaking, level ice, ice resistance, ice load, numerical simulation

AALTO-YLIOPISTO
INSINÖÖRITIETEIDEN KORKEAKOULU

DIPLOMITYÖN
TIIVISTELMÄ

Tekijä: Lauri Kuuliala

Työn nimi: Puolikokeellisen tasaisen jäänmurron simulaatiomallin soveltuvuuden selvittäminen

Päivämäärä: 12.1.2015 Kieli: Englanti Sivumäärä: 7+58

Laitos: Sovelletun mekaniikan laitos

Professuuri: Meritekniikka Koodi: Kul-24

Työn valvoja: Professori Pentti Kujala

Työn ohjaaja: M.Sc. Floris Goerlandt

Työssä toteutettiin eräin muutoksin Biao Sun esittämä puolikokeellinen malli laivan liikkeistä ja jääkuormista jatkuvassa tasaisen jään murrossa. Mallin käytettävyyttä ja herkkyyttä kokeellisesti määritettäville parametreille tutkittiin suorittamalla herkkyysanalyysi sekä vertaamalla mallin antamia tuloksia muihin menetelmiin ja täysmittakaavassa tehtyihin mittauksiin.

Simulaatiossa käytetään tasaisen jään murtomallia, jossa oletetaan jään murtokuvion olevan riippuvainen jään ja laivan suhteellisesta nopeudesta. Jään oletetaan murtuvan taipumalla ja murtuvien palojen olevan muodoltaan ympyrän sektorin rajaamia. Yksittäisessä rungn ja jään kontaktissa vaikuttavat voimat lasketaan ja näiden perusteella muodostetaan globaalit voimat, jotka vaikutavat laivan liikkeisiin, sekä paikalliset jääkuormat.

Menetelmällä voidaan ennustaa laivan maksiminopeutta, jäävastusta ja jääkuormia erilaisissa jääolosuhteissa. Tulosten havaittiin olevan herkkiä suhteessa mallin empiiristen parametrien arvoille. Malli käyttäytyi epävakaasti joillakin parametrien arvojen yhdistelmillä.

Yleisesti ottaen ennustetut nopeudet, vastus ja kuormat olivat järkevällä tasolla.Tuloksissa oli kuitenkin huomattavaa hajontaa johtuen empiiristen parametrien arvojen valinnasta.

Avainsanat: Jäänmurto, tasainen jää, jäävastus, jääkuorma, numeerinen mallinnus

Preface

I would like to thank professor Pentti Kujala not only for supervising this thesis, but also for the opportunity of working for the Ship Laboratory during my thesis. Apart from financial security, this work has halped me to relate my studies to their applications and taught me much about engineering and science.

This thesis was funded through the JOULES-project and the funding is gratefully aknowledged.

I would also like to thank Floris Goerlandt for his invaluable support on the thesis project as my thesis advisor. His comments guided me into the right path in approaching the model and helped me to focus the work.

Also other people working in the laboratory helped me with advice and comments. At least Mikko Suominen, Otto Puolakka and Tommi Mikkola deserve to be mentioned.

Justin Champion helped with language issues. I am grateful for this help and take full blame for any remaining mistakes.

My wife, Petra, was great overall. Thank you.

Otaniemi, 12.1.2015

Lauri Kuuliala

Contents

Symbols

$\mathbf{A}$	Added mass matrix
A	Contact area
$\mathbf{B}$	Damping matrix
B	Breadth of waterline
$\mathbf{C}$	Hydrostatic restoring matrix
C_b	Volumetric block coefficient
C_l, C_v and C_f	Empirical models of the ice-breaking model
E	Strain modulus
$\mathbf{F}$	Force vector
F_c	Magnitude of crushing force
F_H	Magnitude of horizontal force due to ice contact
F_V	Magnitude of vertical force due to ice contact
f_H	Magnitude of horizontal frictional force due to ice cntact
f_V	Magnitude of vertical frictional force due to ice contact
h_i	Thickness of ice
I_{zz}	Moment of inertia about the z-axis
L	Length of waterline
l_c	Characteristic length of ice
$\mathbf{M}$	Mass matrix
m	Mass
P_f	Bearing capacity of an ice wedge
R	Breaking radius of ice
$\mathbf{r}$, $\dot{\mathbf{r}}$ and $\ddot{\mathbf{r}}$	Position, velocity and acceleration vector
T	Draught
T_b	Bollard pull
T_{net}	Net thrust
v_{ow}	Open water speed
v^{rel}	Relative velocity between hull and ice
v_t^{rel} and v_n^{rel}	Component of relative velocity tangential and normal to hull-ice contact
w_p	Apparent width of hull-ice contact
w_c	Actual width of hull-ice contact
X, Y and Z	Coordinates in the global coordinate system
X_G and Y_G	Coordinates of the center of gravity of the ship
x, y and z	Coordinates in the ship coordinate system
α	Entrance waterline angle
μ	Coefficient of friction
ν	Poisson's ratio
ψ	Heading of the ship or hull normal angle at bow
ϕ	Flare angle at bow
ρ_i	Density of ice
ρ_w	Density of water
σ_c	Crushing strength
σ_f	Bending strength
θ	Opening angle of ice wedge

1 Introduction

1.1 Background

Navigation in ice-covered waters is practiced in the Arctic waters and in the Baltic Sea. There is also some activity in the Antarctic waters related to the supply of scientific outposts. Arctic waters contain a significant portion of the unused hydrocarbon resources making operations pertaining to exploration and drilling of oil and gas fields economically important. Due to the shrinking of the Arctic ice cover, the Northern Sea Route along northern parts of Russia between Europe and Asia has become more viable as a transport route.(Kujala and Riska 2010)

The Baltic is the only area with a significant and established winter navigation system for merchant shipping. The Baltic ice season starts in October - November and ends in the end of May when the last ice melts in the northern tip of the Bothnian Bay. The ice cover usually starts to break up in April. The extent of the ice cover is typically greatest from January to March (Vainio and Lumiaro 2014). The length and severity of ice winters vary greatly in different parts of the Baltic Sea. The Finnish Meteorological Institute (FMI) classifies ice winters based on the extent of the ice cover from very mild to very severe using a five-tiered scale. During a normal ice winter the Gulf of Bothnia, Gulf of Finland and northern parts of Baltic Proper are ice-covered. In mild winters the Bothnian Bay and coastal areas of the Bothnian Sea as well as the Gulf of Finland are covered in ice. During the most severe winters the ice-cover extends to Kattegat and even Skagerrak, leaving most of the Baltic Sea covered in ice. The ice season is longest in the Bothnian Bay and eastern parts of the Gulf of Finland.(Vainio and Lumiaro 2013)

Maritime transportation is vital to the Finnish economy. In 2012, 89% of the tonnage of Finnish foreign trade comprised of maritime transportations.(Trafi 2014) As all Finnish ports are ice-bound in the winter except for the most mild winters, a system for winter navigation is important. Knowledge concerning navigation in ice is important for designing ice-going ships for the merchant marine and developing the supporting systems including ice-breakers and traffic restrictions.

Navigation in ice imposes stricter requirements to propulsive power and structures compared to ships designed purely for open water operations (Kujala and Riska 2010). Model testing is widely used in design of ice-going vessels but it is expensive and time consuming. If different alternatives can be compared using simulations prior to model testing, time and expense can be saved in the design phase.

Numerical simulations of ice navigation can adress the problem from different scales and perspectives. Trafficability simulations are concerned with average performance in different ice conditions and do not try to model ship-ice contact accurately, relying instead on semi-empirical formulations for resistance in ice. Route optimization can be coupled with trafficability simulations (Kotovirta et al. 2009). Real-time simulations are useful for training crews and testing the feasibility of different operational doctrines. Commercially available physics-engines can be used for real-time simulations and realistic graphical representation of the surroundings is important for training purposes (Lubbad and Løset 2011). Simulations that do not run in real time

can be used for ship design to investigate the performance and loads on a ship in the design phase.(Valanto 2001; Su 2011) These can be of varying levels of complexity depending on the scope of the simulations.

1.2 Aims and scope of the thesis

A numerical simulation of the performance, motions and ice loads of a ship in the continuous mode of breaking level ice is presented in this thesis. The model is based on the model by Su (2011). The implementation of the method is by the author and some modifications are made to the original simulation model. A model for the crushing of ice that is alternative to that used in the original model is also presented and the results using the different crushing models are compared. In this thesis ship performance is understood to cover resistance and maximum speed in given ice conditions.

The model is semi-empirical and contains three empirical parameters that affect the breaking pattern of ice and the vertical force needed to break ice floes off the parent ice sheet. The effect of these parameters on the predictions of ship performance and loads in ice is the main focus of this thesis. The response of the model to different parameter combinations and inputs is analyzed to gain insight into the stability and usefulness of the simulation method for prediction of ship performance and loads in ice in different cases.

The aims of this thesis are to complete:

- a sensitivity analysis of predicted ship performance and motions to the empirical parameters
- a sensitivity analysis of predicted ice loads to the empirical parameters
- an investigation of the effect of varying ice thickness on the predicted performance and motions
- an investigation of the effect of varying ice thickness on the predicted ice loads
- a comparison of the performance prediction to other empirical methods
- a comparison of the effect of the alternative ice crushing models on the performance and motions predicted by the model
- a comparison of the effect of the alternative ice crushing models on the ice loads predicted by the model
- a comparison of simulated and full-scale results of ice loads acting on the waterline of MT Uikku.

A brief description of ice conditions relevant to navigation and ice breaking is given in chapter 2. Extant simulations of ship performance and loading in ice are outlined in chapter 3. The simulation method and implementation of the method are presented in chapter 4 alongside the modifications made to the original simulation

method. Test cases selected for the sensitivity analysis are presented in chapter 5 and the full-scale data used for validation is presented in chapter 6. Simulation results of selected cases are presented in chapter 7 and the validity of the method and the results are discussed in chapter 8.

2 Ice conditions and ice breaking process

2.1 Ice conditions

Sea ice is formed as level ice when the seawater reaches its freezing temperature and ice crystals start to form around impurities in the water close to the water surface. Ice crystals are buoyant and rise to the surface where they are consolidated to form rind ice. This granular rind ice can reach a thickness of five centimeters. After rind ice has formed, ice starts to grow downwards and forms columnar crystals. Depending on prevailing weather conditions during ice formation, the level ice sheet can be broken and re-frozen several times, resulting in a heterogenous structure.(Weeks 2010)

Level ice stays intact over the winter only near the shoreline where the movement of ice is constrained by land. Further away from shores, ice deforms due to the motions of the ice field forming leads, ice floes, brash ice, rafted ice and ice ridges. The movement of the ice field is governed by winds and currents and the internal friction of the ice field. Due to the dynamics of the ice field, the concentration of sea ice can vary from full coverage to open water. The ice cover is furthermore deformed by vessel traffic. Ice channels form where ships navigate and can be closed by moving ice. Ice channels consist of ice rubble that can be several meters deep if the channel is navigated for a long time. Ice formation is ongoing in the channels if air temperature is below the freezing temperature of water and the ice rubble can be consolidated if the channel is unused for some time.(Kujala and Riska 2010)

Rafted ice forms when a moving ice sheet is deflected on top or under another ice sheet. The sheets forming rafted ice can also be bonded by freezing if they are stationary relative to each other for a sufficiently long time. When the frictional forces caused by rafting reach the buckling treshold of the ice cover the ice starts to fail by buckling and subsequently bending, forming pressure ridges. Ridges consist of piled ice floes and can reach depths of over ten meters. In older ridges a consolidated layer is formed below the waterline. Ridged ice and old channels can constitute a significant hindrance to vessel operations in ice.(Lensu 2003)

Level ice is not the most common ice condition encountered by ships operating in winter nor is it the most difficult for navigation. However, ice conditions are typically easier to define in level ice than in other ice conditions and subsequently the performance of a ship in level ice is often set as the acceptance criterion of an ice-going ship in ship contracts. Level ice loads are significant in considering structural demands of a ship as they are typically greater that loads caused by ice rubble.(Kujala and Riska 2010)

2.2 Ice breaking process

The resistance of a ship in ice is the amount of energy consumed per unit distance traveled, that is the average force resisting the motion of the ship (Enkvist 1972). Different phenomena contribute to ice resistance and ice loads depending on the ice conditions. Crushing and breaking ice by bending, displacing broken ice pieces, ice rubble and water all contribute to the total resistance. Displacing ice rubble can

dominate resistance in ridges and ice channels while in level ice crushing and bending of ice are the major sources of resistance.

Breaking of level ice can be presented ideally as a cyclical process. At the onset of a contact ice is crushed locally. As the ship progresses further into the ice field, frictional forces develop in addition to the crushing force. Because the hull is sloped at the bow area, these forces have a significant vertical component. Radial cracks start to propagate from the contact and they are connected by a circumferential crack when the vertical force reaches the loading capacity of the ice wedges formed by the radial cracking. The broken ice pieces are turned tangential to the hull and submerged by the motion of the ship. The pieces finally slide along the hull untill they are cleared or milled by the propeller.(Enkvist 1972; Yamaguchi et al. 1997) In the continuous mode of ice breaking there are no significant heave, trim or heeling motions as the inertial forces break the ice (Kujala and Riska 2010). Continuous mode of ice breaking is only possible in relatively thin ice, such as that encountered in the Baltic Sea.

In real icebreaking situations new contacts are formed continually and not all contacts lead to bending failure of ice. Especially in the midship or shoulder areas where the frame angles are smaller than at the bow, contacts may lead to only crushing or also to shearing or buckling failure of the ice, depending on the relative motion of the ice and ship. The stress field in the ice is affected also by the horizontal forces in addition to the vertical forces and this has an effect on the crack propagation in ice. Sea ice is anisotropic and often unhomogenous and several contacts may have significant interactions. The motions of the ice floe must also be considered if the ice being broken is not landfast.

Rotation of broken ice pieces can cause significant slamming loads on the hull in high speeds and if sea water can not fill the void between a broken ice piece and the hull of the ship, ventilation occurs. Ventilation increases the hydrostatic force that presses the ice piece against the hull, increasing the resistance component caused by sliding of the broken ice pieces along the hull.(Kämäräinen 2007)

The shape of the hull has a big influence on the relative importance of the different components of ice resistance as well as on the overall resistance in ice. The vertical force that bends ice is dependent on the shape of the bow, as is the breaking pattern of ice as it determines the frequency and location of the ice contacts. The size and shape of the broken ice pieces is influenced by the local shape of the hull on the contact.(Enkvist 1972; Yamaguchi et al. 1997). The underwater shape of the hull also affects resistance in ice as the broken ice pieces follow roughly the buttock lines of the hull before they are cleared.(Kujala and Riska 2010)

3 State of art of simulations of level ice breaking

Many semi-empirical formulas for resistance in level ice have been proposed. Those derived by Enkvist (1972) and Lindqvist (1989) have been influental. A modified version of the Lindqvist method has been presented by Riska et al. (1997)

The problem of modeling a single ice breaking event has been approached analytically by using plate and beam theory. Nevel (1965) derived solutions for a semi-infinite plate on an elastic foundation and a wedge on an elastic foundation in 1968 (Nevel 1968). These papers considered ice loaded vertically by a concentrated loading. The investigated failure mode was bending. In 1979, Nevel included horizontal forces and buckling into the analysis of a wedge on an elastic foundation (Nevel 1979).

Norman investigated a three degree of freedom model of ship motions and breaking pattern in ice in the continuous mode of ice breaking. He assumed the forces to be symmetrical about the xz - plane of the ship leaving surge, heave and pitch as the relevant motion components. The breaking pattern is assumed based on full scale data and the load needed to cause bending failure of ice is based on plate theory and the work of Nevel presented in the previous paragraph.(Norman 1980)

Valanto (2001) developed a numerical model for resistance and loads at waterline of a ship advancing with constant velocity in level ice. The flow around the ship is modeled using a potential flow model and out of plane stresses of the ice cover are modeled based on contact forces and the pressure field caused by the ship. The breaking pattern is not pre-defined but crack propagation is modeled by tracking points in which the principal stress on the top of the ice cover exceeds the bending strength of ice. Broken ice floes are tracked untill they have turned parallel to the hull plating and slamming loads from rotation are also modeled. After rotation submersion and sliding resistance is modeled using relevant parts of the Lindqvist resistance formula. Valanto also analyzed the spatial distribution of loads at the waterline.

Wang (2001) proposed a semi-empirical method for calculating ice-breaking forces and the breaking pattern for a conical structure. The model was used by Su (2011) in his simulation of the planar motions and ice loads on ships operating in level ice. This model was expanded to six degrees of freedom by Tan et al. (2013). Zhou (2012) expanded Su's planar motion model by adding a more detailed handling of the submersion and pile-up of broken ice when he considered stationkeeping of moored vessels in drifting ice.

A discrete element method code for ice-related problems, DECICE, was used by Lau et al. (2006) to simulate planar motion a ship manouvering in level ice. Ice was modeled by using 3D plate bending elements and compressive, shear, tensile and flexural modes of failure were modeled.

Sawamura et al. (2009) presented a method to calculate the breaking pattern of a ship advancing in level ice as well as the breaking forces. Bending failure of the ice sheet is the main focus of the work. Dynamic effects are modeled by using a fluid-ice interacion finite element analysis. Forces resulting from rotating, submerging and sliding broken ice pieces are omitted in the model which calculates the motions only

Table 1: A summary of simulations of continuous-mode icebreaking.

Source	DoF	Ice breaking model	Modeled parts of the ice breaking process	Modeled phenomena
Norman (1980)	surge, heave, pitch	analytic	crushing, bending, rotation, submersion, sliding	Resistance and motions
Valanto (2001)	surge	analytic	crushing, bending, rotation, (submersion by Lindqvist formula)	Resistance and loads
Lau et al. (2006)	surge, sway, yaw	FEM	crushing, shearing, bending, rotation, submersion, sliding	Resistance and motions
Sawamura et al. (2009)	surge	FEM	bending	Resistance
Su (2011)	surge, sway, yaw	semi-empirical	bending, crushing (submersion by Lindquist formula)	Resistance, motions and loads
Lubbad and Løset (2011)	surge, sway, yaw	analytic, real-time	crushing, bending, rotation, submersion, sliding	Resistance and motions
Tan et al. (2013)	surge, sway, pitch, heave, trim, yaw	semi empirical	bending, crushing (submersion by Lindquist formula)	Resistance, motions and loads

in the surge direction.

Lubbad and Løset (2011) presented a real-time numerical simulation model in three degrees of freedom. The ice breaking model is based on the theory of a semi-infinite plate resting on an elastic foundation which is solved analytically for a distributed load. Only bending failure is modeled but the broken ice pieces are tracked and may be rebroken during contacts with the ship or each other. The deflection and stresses in the ice floes are calculated by a commercial finite element method solver.

Berglund (2012) introduced an ice fracture model to be used in simulations of winter navigation. A quasi-static crack-propagation model is used to distribute collision energy. The shape and size of the broken ice pieces is not predetermined. The broken ice pieces are tracked and their interaction with each other and the hull of the ship is modeled.

A summary of simulations of continuous mode of icebreaking is given in table 1.

4 Outline of the simulation method

Planar motion of a ship operating in the continuous mode of icebreaking as well as the loads caused by ice contacts are simulated by the method. Given initial conditions and properties of ship and ice field, the method produces simulated time histories of the position, velocity and acceleration of the ship as well as magnitude and location of ice loads on the waterline.

The three degrees of freedom equations of motion are solved in time domain for the ship which is treated as a rigid body. The excitation is composed of ice contact and submersion forces as well as propeller thrust and hydrodynamic forces. Newmark's method is used for the numerical integration. The geometry of the ice field is altered when bending failure of the ice field is detected.

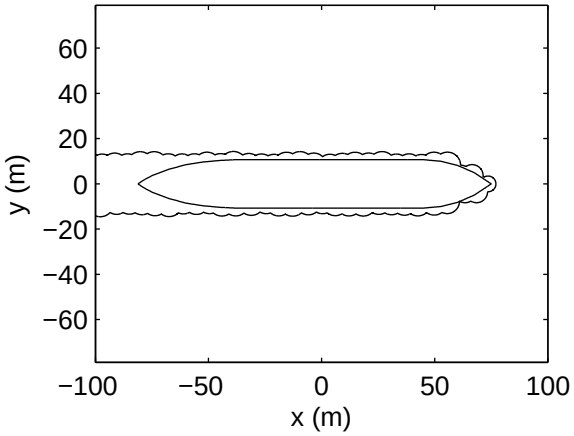

Figure 1: Polygons describing the waterline of the ship and edge of the icefield.

The ice field and ship are modelled by discretized geometries of the ice edge and waterline of the ship as shown in figure 1 as well as sets of parameters describing the mechanical properties of the ice cover and relevant characteristics of the ship. Contact between the ice field and ship is determined for each time step by deciding the extent of overlap of the polygons describing the ice field and hull waterline geometries. Magnitudes and directions of contact forces are determined as well as possible failure of the ice field. The only considered failure modes of ice are bending and crushing. The contact forces are combined with ice submersion and sliding forces calculated with the formula by Lindqvist (1989) as well as hydrodynamcl forces and thrust to compile the excitation for solving the equations of motion for the next time step. Broken ice is cleared from the ice field geometry at the end of each time step.

The coordinate systems employed in the model are described in section 4.1 and the ship and ice field models are described in sections 4.2 and 4.3 respectively. The

main function of the simulation program is the solver for the equations of motion described in section 4.4. The excitation force vector is the sum of a hydrodynamic force vector, net thrust and ice force vector. The modeling of the contact forces is described in section 4.5 and the modeling of submersion and sliding forces is described in section 4.6. The hydrodynamic forces and net thrust are calculated in separate functions described in sections 4.7 and 4.8.

4.1 Coordinate systems

Two coordinate systems are used in the simulation.The position of the center of gravity of the ship is solved in a global coordinate system and the contact forces are solved in a body-fixed coordinate system moving with the vessel. The axes of the coordinate systems are denoted by X, Y and Z for the global system and by x, y and z for the body-fixed coordinate system.

The XY-plane of the global coordinate system lies on the still water level. The system is right-handed and the Z-axis points down. The origin of the body-fixed coordinate system is on the XY-plane on the projected location of the center of gravity of the vessel. The x-axis points towards the bow, y-axis to starboard and z-axis down.

Position vector $\mathbf{r}$ connects the origins of the global and body-fixed coordinate systems. The heading of the ship denoted by ψ is the angle between the X- and x-axes.

Points can be transformed from the body-fixed coordinate system to the global system by

$$\begin{Bmatrix} x \\ y \\ \psi \end{Bmatrix} = \frac{1}{\cos^2\psi + \sin^2\psi} \begin{bmatrix} \cos\psi & \sin\psi & 0 \\ -\sin\psi & \cos\psi & 0 \\ 0 & 0 & 1 \end{bmatrix} \begin{Bmatrix} X \\ Y \\ \psi \end{Bmatrix} + \begin{bmatrix} \cos\psi & \sin\psi & 0 \\ \sin\psi & -\cos\psi & 0 \\ 0 & 0 & 0 \end{bmatrix} \begin{Bmatrix} X_G \\ Y_G \\ 0 \end{Bmatrix} \tag{1}$$

and from the global coordinate system to the body-fixed system by

$$\begin{Bmatrix} X \\ Y \\ \psi \end{Bmatrix} = \begin{bmatrix} \cos\psi & -\sin\psi & 0 \\ \sin\psi & \cos\psi & 0 \\ 0 & 0 & 1 \end{bmatrix} \begin{Bmatrix} x \\ y \\ \psi \end{Bmatrix} + \begin{Bmatrix} X_G \\ Y_G \\ 0 \end{Bmatrix}. \tag{2}$$

The transformation matrix in equation 2 is also used to convert velocities between the different coordinate systems.(Salonen 2003)

4.2 Ship model

The geometry of the ship is modeled by a discretized waterline of the floating plane. Each discretization point of the waterline is assigned an inward-pointing normal unit vector and an aft-pointing tangential unit vector that are used to orient the forces

Table 2: Variables used to model the ship in the simulation.

Variable	Symbol	Needed for
Length of waterline	L	Submersion resistance and hydrodynamic derivatives
Breadth at waterline	B	Submersion resistance and hydrodynamic derivatives
Draught	T	Submersion resistance and hydrodynamic derivatives
Volumetric block coefficient	C_b	Hydrodynamic derivatives
Entrance waterline angle	α	Submersion resistance
Flare angle at bow	ϕ	Submersion resistance
Hull normal angle at bow	Ψ	Submersion resistanc.
Mass of displacement	m	Equations of motion
Moment of inertia about z-axis	I_{zz}	Equations of motion.
Added mass matrix	$\mathbf{A}$	Equations of motion
Damping matrix	$\mathbf{B}$	Equations of motion
Bollard pull	T_b	Net thrust
Open water speed	v_{ow}	Net thrust

Table 3: Variables used for the modeling of ice in the simulation.

Variable	Symbol	Needed for
Coefficient of friction	μ	Contact forces, submersion force.
Poisson's ratio	ν	Characteristic length of ice.
Strain modulus	E	Characteristic length of ice.
Crushing strength	σ_c	Crushing force.
Bending strength	σ_f	Determination of bending failure.
Thickness	h_i	Contact area, submersion force, characteristic length of ice.
Density of ice	ρ_i	Submersion force.
Density of water	ρ_w	Submersion force.

caused by ice contacts. Also, flare angles are assigned for the points. The flare angles are used in dividing the contact forces into vertical and horizontal components and determining contact areas. The variables of the ship model are presented in table 2.

4.3 Ice model

The geometry of the ice field is discretized and represented as a polygon. Ice properties are set as constants for the whole ice field. It is assumed that ice is isotropic and homogeneous. A list of the ice properties with descriptions of their use is presented in table 3.

4.4 Solver for equations of motion

The equations of motion can be written as

$$(\mathbf{M} + \mathbf{A})\ddot{\mathbf{r}}(t) + \mathbf{B}\dot{\mathbf{r}}(t) + \mathbf{C}\mathbf{r}(t) = \mathbf{F}(t), \tag{3}$$

where t is time, $\mathbf{M}$ is the mass matrix, $\mathbf{A}$ is the hydrodynamic added mass, $\mathbf{B}$ is damping and $\mathbf{C}$ is the hydrostatic restoring forces. $\mathbf{r}$ is the position vector of the center of gravity of the ship in the global coordinate system and $\mathbf{F}$ is the excitation force.

Hydrodynamic restoring forces are zero in planar motion and the excitation caused by ice is dependent on position and velocity in this model, leading to equations of motion of the form

$$(\mathbf{M} + \mathbf{A})\ddot{\mathbf{r}}(t) + \mathbf{B}\dot{\mathbf{r}}(t) = \mathbf{F}(\mathbf{r}(t), \dot{\mathbf{r}}(t)). \tag{4}$$

The simulation is performed in three degrees of freedom, namely surge, sway and yaw motions, and lateral symmetry of the ship is assumed. Linear manouvering theory is used to obtain the terms of the added mass and damping matrices as explained in more detail in chapter 4.7. The mass matrix and position vector are of the form:

$$\mathbf{M} = \begin{bmatrix} m & 0 & 0 \\ 0 & m & 0 \\ 0 & 0 & I_{zz} \end{bmatrix} \quad \text{and} \quad \mathbf{r} = \begin{bmatrix} X_G \\ Y_G \\ \Psi \end{bmatrix}$$

In the above, m is the mass of the ship, I_{zz} is the moment of inertia about the z-axis, X_G and Y_G are the coordinates of the center of gravity of the ship and Ψ is the heading of the ship.

The excitation is

$$\mathbf{F} = \begin{bmatrix} F_{Xi} + T_{net} \\ F_{Yi} \\ M_{zzi} \end{bmatrix}, \tag{5}$$

where F_{Xi}, F_{Yi} and M_{zzi} are forces and moments caused by ice contacts and submersion and sliding of broken ice pieces and T_{net} is net thrust.

The equations of motion are solved using Newmark's method which in the general form at time step $k+1$ is

$$\dot{\mathbf{r}}(t_{k+1}) = \dot{\mathbf{r}}(t_k) + (1-\lambda)\ddot{\mathbf{r}}(t_k)\delta t + \lambda\ddot{\mathbf{r}}(t_{k+1})\delta t \tag{6}$$

$$\mathbf{r}(t_{k+1}) = \mathbf{r}(t_k) + \dot{\mathbf{r}}(t_k)\delta t + \left(\frac{1}{2} - \beta\right)\ddot{\mathbf{r}}(t_k)\delta t^2 + \beta\ddot{\mathbf{r}}(t_{k+1})\delta t^2 \tag{7}$$

The terms λ and β are determined by requirements related to accuracy and stability. The only usable value for λ is $1/2$ as other values lead to unphysical numerical damping. Setting $\beta = 1/6$ leads to linearily varying acceleration over the time step. (Newmark 1959) With this choice of the parameters, equations 6 and 7 become

$$\dot{\mathbf{r}}(t_{k+1}) = \dot{\mathbf{r}}(t_k) + \frac{1}{2}\ddot{\mathbf{r}}(t_k)\delta t + \frac{1}{2}\ddot{\mathbf{r}}(t_{k+1})\delta t \tag{8}$$

$$\mathbf{r}(t_{k+1}) = \mathbf{r}(t_k) + \dot{\mathbf{r}}(t_k)\delta t + \frac{1}{3}\ddot{\mathbf{r}}(t_k)\delta t^2 + \frac{1}{6}\ddot{\mathbf{r}}(t_{k+1})\delta t^2. \tag{9}$$

This leads to continuity in acceleration, velocity and displacement.(Newmark 1959) The accelerations at time step $k+1$ are

$$\ddot{\mathbf{r}}(t_{k+1}) = (\mathbf{M} + \mathbf{A})^{-1}\mathbf{F}(t_{k+1}) \tag{10}$$

By inserting the right side of equation 10 in equations 8 and 9 and combining equations, the method can be presented in the form (Su 2011)

$$\mathbf{r}(t_{k+1}) = \left(\frac{6}{\delta t^2}(\mathbf{M} + \mathbf{A}) + \frac{3}{\delta t}\mathbf{B}\right)^{-1}(\mathbf{F}(t_{k+1}) + (\mathbf{M} + \mathbf{A})\mathbf{a}_k + \mathbf{B}\mathbf{b}_k), \tag{11}$$

where $\mathbf{a}_k$ and $\mathbf{b}_k$ are constant terms based on the position, velocity and acceleration at the previous time step given by

$$\mathbf{a}_k = \frac{6}{\delta t^2}\mathbf{r}(t_k) + \frac{6}{\delta t}\dot{\mathbf{r}}(t_k) + 2\ddot{\mathbf{r}}(t_k) \tag{12}$$

$$\mathbf{b}_k = \frac{3}{\delta t}\mathbf{r}(t_k) + 2\dot{\mathbf{r}}(t_k) + \frac{1}{2}\ddot{\mathbf{r}}(t_k)\delta t. \tag{13}$$

Equation 11 cannot be solved directly because the excitation is dependent on the position and velocity at the time step to be solved. Iteration is performed for each time step where the starting point of position and speed are calculated assuming constant acceleration

$$\mathbf{r}^0(t_{k+1}) = \mathbf{r}(t_k) + \dot{\mathbf{r}}(t_k)\delta t + \frac{1}{2}\ddot{\mathbf{r}}(t_k)\delta t^2 \tag{14}$$

$$\dot{\mathbf{r}}^0(t_{k+1}) = \dot{\mathbf{r}}(t_k) + \ddot{\mathbf{r}}(t_k)\delta t. \tag{15}$$

The iteration is started by calculating excitation with position and velocity given by equations 14 and 15. New value for the position is calculated using equation 11 and velocity is updated using equation 8. These new values are then used to determine excitation for the next iteration round. The iteration is continued untill the change in the excitation from one iteration to the next is small enough. The stopping criterion is

$$\frac{\left\|\mathbf{F}(t_{i+1}) - \mathbf{F}(t_i)\right\|}{\left\|\mathbf{F}(t_i)\right\|} < \varepsilon, \tag{16}$$

where ε is of the order 10^{-3}.

4.5 Modeling of ice contacts

Modeling of ice contacts has the following main phases. Contacts are identified for a given time step and the geometry and position of the contacts are established. The contact forces are then determined based on the contact area and relative velocity of the contact and ice. Finally, the contact forces are divided into vertical and horizontal components.

The breaking radius of each contact is then determined based on the characteristic length of ice and relative normal velocity in the xy-plane. An opening angle of breaking ice is calculated for each contact from the ice geometry and breaking radius. A limit force for bending failure is calculated based on this angle. Bending failure occurs where the vertical contact force exceeds the limit force.

For the purpose of determining excitation, the contact force is reduced in case of bending failure so that the vertical force is set to equal the limit force and the horizontal component of the contact force is modified accordingly. The ice geometry is altered to include the breaking events and the excitation due to ice contacts is calculated as the vector sum of the horizontal contact forces.

The modeling of ice contact mostly follows the method by Su (2011). However the following alterations have been made to the original simulation method:

- Contact areas are not discretized as triangular sub areas. Instead numerical integration is used to determine the area bounded by a polyline with known vertices.

- Ice-breaking radius is not determined based on the average relative velocity between ship and ice at the first and last points of a contact. Rather, the breaking radius is determined based on the relative velocity at the mid-point of contact.

- An alternative method to determine the crushing force at contact is introduced and compared to the original method.

4.5.1 Identification of hull-ice contacts

Any discretization points of the edge of the icefield that lie inside the hull polygon are considered to be in contact with the hull as illustrated in figure 2. Ice nodes that lie inside the hull polygon are determined using an algorithm that supposes that the hull polygon is convex and symmetrical. The vectors containing the coordinates of the nodes of the ice edge geometry are ordered so that subsequent indices of the vectors correspond to neighbouring points of the ice edge. Thus, one contact is comprised of ice nodes inside the hull polygon that have consequtive indices. The length of the contact is the distance from the first to last ice node in the contact.

The number of contacts for a time step is the number of sequences of consecutive ice nodes that are inside the hull polygon. Contacts are idealized as planar areas. For each contact, the area and orientation of the contact plane has to be determined.The orientation of a contact in the xy-plane is determined by the normalized vector sum of the normal vectors of the hull nodes that take part in the contact and the normalized vector sum of the tangential vectors of the nodes. Figure 3 illustrates the determination of the orientation of a contact in the xy-plane. The orientation in the yz-plane is determined by the mean of the flare angles of the hull nodes that take part in the contact. Contact length is the distance between the first and last ice nodes in the contact.

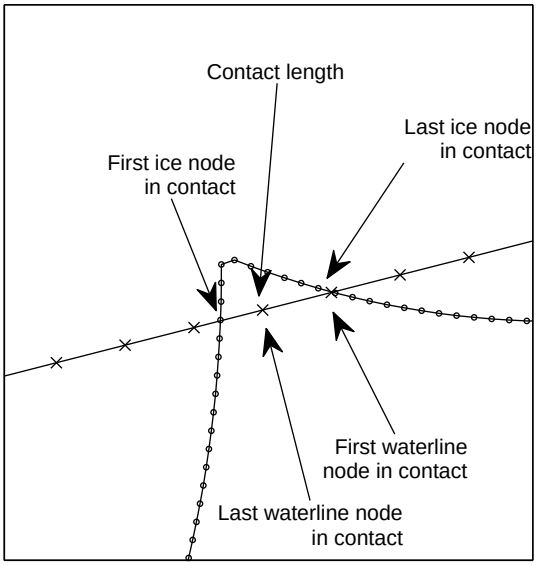

Figure 2: An example of an ice contact. Ice edge and waterline nodes that take part in the contact and the contact area projected in the xy-plane are shown. Contact length is the distance between first and last ice nodes in the contact.

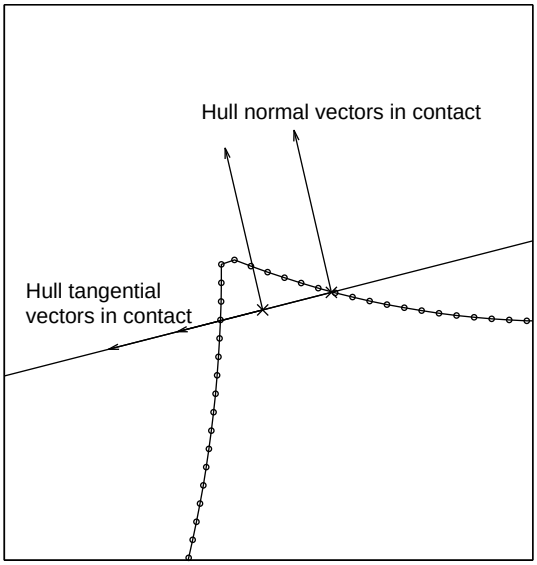

Figure 3: Normal and tangential vectors of the waterplane that detertmine the orientation of the contact in the xy-plane.

For the determination of the contact area, the effect of the flare angle of the contact has to be taken into account. Projected local widths of the contacts are the distances from the span line of the contact to the ice nodes of the contact. The actual widths depend on the local ice thickness and flare angle of the contact by

$$w_c = \begin{cases} w_p \cos\bar{\varphi} & \text{,if} \quad w_p \tan\bar{\varphi} \leq h_i \\ \frac{h_i}{\sin\bar{\varphi}} & \text{,if} \quad w_p \tan\bar{\varphi} > h_i, \end{cases} \tag{17}$$

where w_p is the projected width of the contact and w_c is the corrected width. $\bar{\varphi}$ is the mean of the local flare angles of the contact and h_i is the ice thickness.(Su 2011)

For the purpose of calculating the contact area the ice nodes are moved by distance $w_c - w_p$ in a direction perpendicular to the line spanning between the intersection points of the contact. The contact area is the area of the polygon bounded by the intersection points of waterline and ice edge, hull nodes in the contact and the adjusted ice nodes in the contact. The area is calculated by using numerical integration. Centroids of the contact areas are calculated and used as the location of the contact when excitation is determined..

4.5.2 Modeling of crushing and frictional forces

Crushing is assumed to be the only failure mode prior to bending. Thus, the component of the contact force normal to the contact plane is determined by the force needed to crush the ice. Ice crushing pressure can be estimated based on the nominal contact area by

$$p_c = CA^a, \tag{18}$$

where C is the pressure over 1 m^2, A is the nominal contact area in square meters, a is a negative exponent and p_c is the crushing pressure in megapascals.(Daley 2007) The crushing force is obtained by multiplying the crushing pressure by the nominal contact area, giving

$$F_c = CA^{1+a}. \tag{19}$$

F_c is the ice force normal to the contact plane. In this thesis, crushing strength of ice is used for the value of C and a is set to be -0.4 resulting in the formula for the crushing force to be

$$F_c = \sigma_c A^{-0.6} \tag{20}$$

An alternative formulation for the crushing force is used by Su (2011) where the crushing force is linearly dependent on the contact area and given by

$$F_c = \sigma_c A. \tag{21}$$

Both methods are used in this thesis and the results are compared.

Friction between ice and hull also causes forces tangential to the contact plane. The component of the frictional force tangential to the contact in the xy-plane, f_H affects the excitation force. The component aligned with the vertical plane normal to the contact plane, f_V affects the total vertical force of the contact. The relevant force and relative velocity components are illustrated in figure 4.

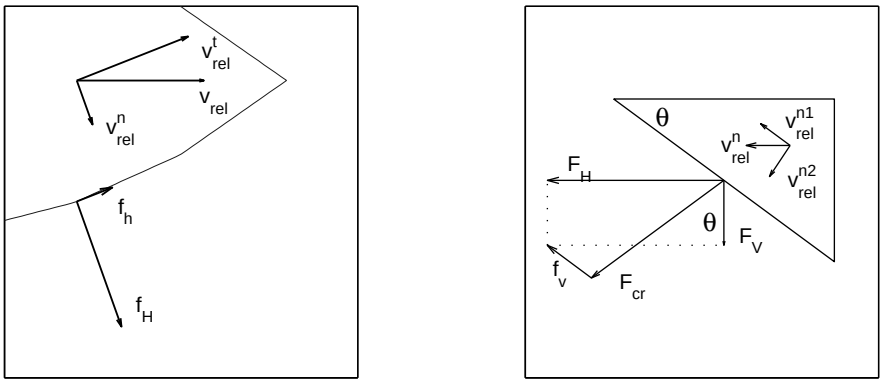

Figure 4: Components of contact force and relative velocity in the xy- (left) and xz-planes (right).

Frictional forces are acting in a direction opposite to the relative motion of the ship hull and ice. The frictional force of a contact has a horizontal and vertical component. The force is divided into the components according to the magnitude of relative velocity components in relation to the total magnitude of relative velocity between ship and ice. The horizontal and vertical contributions of the frictional forces are given by Su (2011) as

$$f_H = \frac{\mu F_c v_t^{rel}}{\sqrt{(v_t^{rel})^2 + (v_{n1}^{rel})^2}} \tag{22}$$

$$f_V = \frac{\mu F_c v_{n1}^{rel}}{\sqrt{(v_t^{rel})^2 + (v_{n1}^{rel})^2}}. \tag{23}$$

Total horizontal and verticall forces in the vertical plane normal to the contact are given by

$$F_H = F_c \sin\varphi + f_V \cos\varphi \tag{24}$$

$$F_V = F_c \cos\varphi - f_V \sin\varphi. \tag{25}$$

4.5.3 Modeling of ice bending failure

The radius of broken ice floes is given by

$$R = C_l l_c (1 + C_v v_n^{rel}), \tag{26}$$

where C_l and C_v are constants, v_n^{rel} is the relative normal velocity of the contact plane and ice and l_c is the characteristic length of ice on water foundation that is assumed to be linearly elastic. Characteristic length of ice is given by

$$l_c = \left(\frac{E h_i^3}{12(1-\nu^2)\rho_w g} \right)^{0.25}. \tag{27}$$

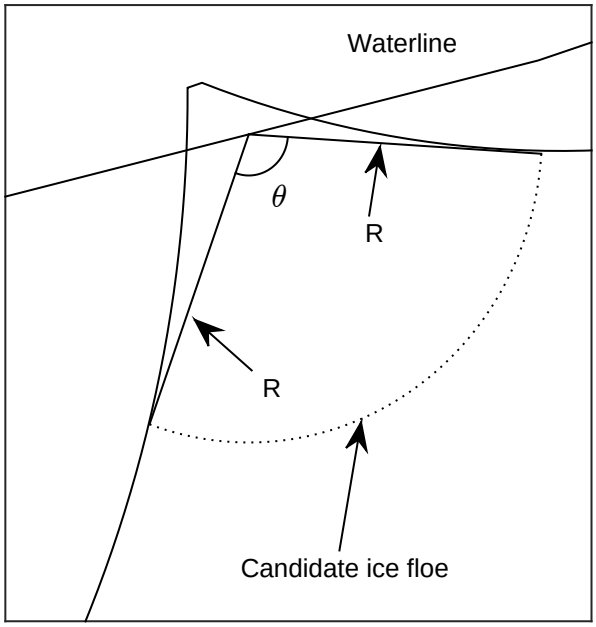

Figure 5: Determination of the opening angle θ of breaking ice floes.

C_l is positive and C_v is negative. The effect of the constants and their selection is discussed further in section 5.

The breaking radii of the contacts determine the opening angle, θ of broken ice floes as shown in figure 5. The opening angle in turn affects the limit force needed for bending failure given by

$$P_f = C_f \left(\frac{\theta}{\pi}\right)^2 \sigma_f h_i^2, \tag{28}$$

where θ is the opening angle of the breaking ice floe, σ_f is the flexural strength of ice and h_i is the thickness of ice. The vertical component of the contact force of a given contact is compared to the limit force of the same contact and if $F_V \geq P_f$, ice fails by bending. In this case f_H, f_V, F_H and F_V are recalculated with $F_c = P_f$ for determination of the excitation force.

After all contacts are resolved, the ice edge geometry is altered to take bending failures into account. All of the contacts are assumed to be independent and all bending failures during a time step are assumed to be simultaneous.

The horizontal components of the contact forces, F_H and f_H, are divided into x- and y-directional components. F_H acts in the direction normal to the contact in the xy-plane and f_H in the direction tangent to the contact in the same plane. Moments are calculated by

$$M_{zzi} = \sum_{j=1}^{n} (x_j F_{yj} + y_j F_{xj}), \tag{29}$$

where x_j and y_j are the coordinates of the midpoint of the ith contact and F_{xj} and F_{yj} the associated x- and y-directional contact forces.

4.6 Submersion forces

The forces caused by the submersion and sliding along the hull of the broken ice pieces is modeled by calculating the submersion resistance component of the ice resistance formula presented by Lindqvist (1989). In the original formulation, submersion resistance has a speed-dependent contribution to the overall ice resistance. In the simulation the submersion resistance has surge and sway components that are obtained by

$$F_{xs} = R_s \left(1 + 9.4 \frac{v^{rel}}{\sqrt{gL_{wl}}}\right) \frac{v_x^{rel}}{v^{rel}} \tag{30}$$

and

$$F_{ys} = R_s \left(1 + 9.4 \frac{v^{rel}}{\sqrt{gL_{wl}}}\right) \frac{v_y^{rel}}{v^{rel}}, \tag{31}$$

where v_x^{rel} and v_y^{rel} are the components of relative velocity between the ice field and ship (Su 2011). R_s is the submersion resistance component calculated according to (Lindqvist 1989).

Lindqvist (1989) makes the assumption that the bottom of an ice-breaking ship is covered by ice for $0.7L$ from the bow. This implies that the resultant force caused by submersion and sliding of broken ice does not act on the center of gravity of the ship. Thus, F_{ys} should cause a yaw-moment. This is however not taken into account in the original method by Su (2011) nor in this thesis. Lindqvist formula does not claim such an accuracy that the longitudinal location of F_{ys} and thus the resulting moment could be determined.

4.7 Modeling of hydrodynamic forces

In the implementation of the model in this thesis, forces due to relative motion of ship and water are not calculated using the strip method, that is used by Su (2011). Instead, a linear approximation of the in-plane motion of a ship and slow motion hydrodynamic derivatives are used and the results are incorporated into the left side of equation 11 as the linear terms of added mass and damping. In this approach it is assumed that the hydrodynamic forces acting on the hull and appendages are linearily dependent on the components of velocity. The y-directional force, Y and moment about the z-axis, N are given by

$$Y = Y_{\dot{v}}\dot{v} + Y_v v + Y_{\dot{r}}\dot{r} + Y_r r \tag{32}$$

and

$$N = N_{\dot{v}}\dot{v} + N_v v + N_{\dot{r}}\dot{r} + N_r r, \tag{33}$$

where for example N_v is the partial derivative of the moment with respect to sway velocity.(Matusiak 2013). $Y_{\dot{v}}$, $Y_{\dot{r}}$, $N_{\dot{v}}$ and $N_{\dot{r}}$ correspond to the first order terms of

added masses of sway and yaw motion and Y_v, Y_r, N_v and N_r correspond to the first order terms of damping of the sway and yaw motions. x-directional added masses are assumed negligible as are added mass and damping components related to the surge motion. X_u is not needed as the net thrust model takes hydrodynamic resistance implicitly into account. This is explained further in section 4.8. The added mass matrix, $\mathbf{A}$, and damping matrix, $\mathbf{B}$, when only the first order terms are taken into account are

$$\mathbf{A} = \begin{bmatrix} 0 & 0 & 0 \\ 0 & Y_{\dot{v}} & Y_{\dot{r}} \\ 0 & N_{\dot{v}} & N_{\dot{r}} \end{bmatrix} \tag{34}$$

$$\mathbf{B} = \begin{bmatrix} 0 & 0 & 0 \\ 0 & Y_v & Y_r \\ 0 & N_v & N_r \end{bmatrix} \tag{35}$$

Linear seakeeping theory used in this thesis for hydrodynamic forces is valid only for small drift angles. In cases where drift exceeds 10 degrees another method for determining hydrodynamic forces is needed.(Matusiak 2013) In any case more accurate results can be obtained by using for example computational hydrodynamics if a 3D-model of the hull is available.

The slow motion derivatives can be determined by model tests or computational fluid dynamics. There is also a method based on regression of results of model tests to approximate the non-dimensional forms of the hydrodynamic derivatives. This method is used for the simulations in this thesis because it was not practicable to obtain more accurate results. The non-dimensional hydrodynamic derivatives based on the main dimensions are given by equations 36-43 (Matusiak 2013).

$$Y'_{\dot{v}'} = -\pi(T/L)^2(1 + 0.16C_B B/T - 5.1(B/L)^2) \tag{36}$$
$$Y'_{\dot{r}'} = -\pi(T/L)^2(0.67B/L - 0.00033(B/T)^2) \tag{37}$$
$$N'_{\dot{v}'} = -\pi(T/L)^2(1.1B/L + 0.0003341B/T) \tag{38}$$
$$N'_{\dot{r}'} = -\pi(T/L)^2(1/12 + 0.0176C_b B/T - 0.33B/L) \tag{39}$$
$$Y'_{v'} = -\pi(T/L)^2(1 + 0.4C_B B/T) \tag{40}$$
$$Y'_{r'} = -\pi(T/L)^2(-0.5 + 2.2B/L - 0.08B/T) \tag{41}$$
$$N'_{v'} = -\pi(T/L)^2(0.5 + 2.4T/L) \tag{42}$$
$$N'_{r'} = -\pi(T/L)^2(0.25 + 0.039B/T - 0.56B/L) \tag{43}$$

The non-dimensional hydrodynamic derivatives are calculated before the start of the simulation and dimensional derivatives are calculated for each time step based on the instantaneous velocity. The non-dimensional coefficients are dimensionalized by density of water, length of the ship and surge velocity (Matusiak 2013).

4.8 Thrust modeling

The concept of net thrust is used in modeling the thrust in the simulation. Net thrust is the amount of thrust available to overcome resistace in addition to open

Table 4: Values of K_E for the estimation of bollard pull.(Kujala and Riska 2010)

	Controllable pitch	Fixed pitch
Single propeller	0.78	0.87
Twin propeller	0.98	1.09
Triple propeller	1.12	1.24

water resistance at a given speed. When the concept of net thrust is used to model propulsion forces, open water resistance is not explicitly modeled. At zero speed the net thrust is the bollard pull and at open water speed it is zero. If no data about bollard pull is available it can be estimated based on propulsive power and propeller diameter by

$$T_B = K_E(PD)^{2/3}. \tag{44}$$

K_E is an empirical factor, P is the power in kilowatts, D is the propeller diameter in meters and T_B is bollard pull in kilonewtons. Values for K_E are given in table 4.(Kujala and Riska 2010)

Net thrust can be related to bollard pull by using an approximative quadratic formula

$$T_{NET} = T_B \left(1 - \frac{v}{3v_{ow}} - \left(\frac{2v}{3v_{ow}}\right)^2\right). \tag{45}$$

v is the instantaneous surge speed and v_{ow} is the maximum open water speed of the ship.(Kujala and Riska 2010) The formula gives a net thrust of more than bollard pull for negative speeds and negative thrust for speeds exceeding open water speed. In the simulation negative thrust is treated as zero thrust and thrust over bollard pull as equal to bollard pull.

5 Sensitivity analysis

Test cases selected for the sensitivity analysis of the simulation model are explained in this chapter. All the cases for the sensitivity analysis are simulated with similar ice properties and initial conditions. All the cases start with the ship encountering the ice edge perpendicular to the direction of motion of the ship. The initial speed of the ship is 6 m/s and the ice thickness is 0.4 m. The ice properties are summarized in table 5 and the selected parameter combinations in table 6.

Table 5: Ice properties used in the sensitivity analysis.

σ_f	0.58 MPa
σ_c	2.3 MPa
E	8 GPa
μ	0.15
ν	0.33
ρ_w	1020 kg/m^3
ρ_i	980 kg/m^3

5.1 Selection of values of the empirical coefficients

The simulated breaking pattern and load levels are influenced by three empirical coefficients, C_l, C_v and C_f. The breaking radius is influenced by C_l and C_v and C_f sets the level of the limit force for bending failure of ice. Justification for the selection of the values of these parameters for the sensitivity analysis is given in this section.

5.1.1 Selection of values for C_l and C_v

Equation 10 can be rearranged to give the breaking radius relative to the characteristic length of ice

$$R/l_c = C_l C_v v_n^{rel} + C_l \tag{46}$$

The term $C_l C_v$ is negative meaning that R/l_c decreases with increasing relative normal velocity. C_l is the upper limit for R/l_c at zero relative normal velocity. C_v together with C_l determines the influence of relative velocity on R/l_c. Figure 6 illustrates the effect of the empirical parameters on R/l_c.

Enkvist (1972) lists various calculated and test results for R/l_c that are summarized in table 7. Based on the values presented in table 7, the range of R/l_c should not be greater than 1 to 0.3 in the expected range of relative normal velocities. Assuming surge velocity of 6 m/s and maximum angular velocity of 0.05 rad/s the relative normal velocities range from close to 0 m/s to little under 7 m/s depending on the location of contact. Even though the full-scale tests do not indicate the upper bound to be more than 0.7 there is no data available on the speed range of the full scale tests. However, the ratio of 1 in the model scale tests is reported to have occured at low speeds.

Table 6: Combinations of the empirical parameters of the model used for the sensitivity analysis.

C_v	C_l	C_f
-0.08	1.0	3.0
-0.09	1.0	3.0
-0.10	1.0	3.0
-0.11	1.0	3.0
-0.12	1.0	3.0
-0.08	1.0	3.2
-0.09	1.0	3.2
-0.10	1.0	3.2
-0.11	1.0	3.2
-0.12	1.0	3.2
-0.08	1.0	3.5
-0.09	1.0	3.5
-0.10	1.0	3.5
-0.11	1.0	3.5
-0.12	1.0	3.5
-0.08	0.8, 0,9, 1.0, 1.1	3.8
-0.09	0.8, 0,9, 1.0, 1.1	3.8
-0.10	0.8, 0,9, 1.0, 1.1	3.8
-0.11	0.8, 0,9, 1.0, 1.1	3.8
-0.12	0.8, 0,9, 1.0, 1.1	3.8

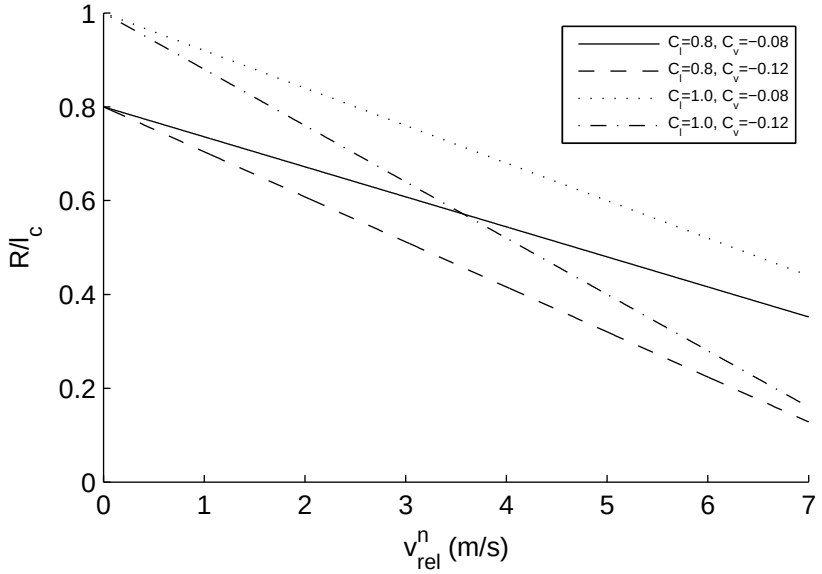

Figure 6: Speed dependency of the breaking radius of ice normalized by the characteristic length of ice with different values of C_l and C_v.

Table 7: Calculated and tested values for R/l_c.(Enkvist 1972)

R/l_c	Notes
0.8	Analytical for cusp, plate theory.
0.3 - 0.6	Cusp test.
0.5 - 1.0	Model test.
0.3 - 0.7	Full-scale test.

Other factors than relative velocity at the point of contact also affect the test results. In experimental work the characteristic length of ice is very much an approximation as the properties of ice are difficult to measure and can vary significantly over short distances. Thus, it is difficult to say exactly what the range of breaking radii should be in the simulated results. However, typical values around 0.5 should be reasonable in light of table 7.

Wang uses equation 10 for interaction of a conical structure and an ice sheet with constant velocity of 0.7 m/s. The relative velocity is much lower than in icebreaking situations and the ice is broken upwards which could affect the range and speed dependency of breaking radii. Wang uses values of $C_l = 0.32$ and $C_v = -0,14$ in her simulations if similar definitions are used as in this thesis.(Wang 2001) These values produce too low values for R/l_c for a ship breaking ice at higher speeds and it would seem that the parameters are dependent on the application case. Specifically, the value chosen for C_l is definitely too low to produce the results expected based on the data in table 7.

The value of C_l should be close to one to produce breaking radii consistent with known results. The values of C_l chosen for the sensitivity analysis are 0.8, 0.9, 1 and 1.1. The choice of values of C_v is more difficult to justify but -0.08, -0.09, -0.10, -0.11 and -0.12 are chosen for the analysis.

5.1.2 Selection of values of C_f

The coefficient C_f sets the limit force needed for bending failure of an ice wedge with a given opening angle. Su (2011) states that values from around 1 to 4.5 have been reported in publications by Kashtelian and Nguyen et al. Kashtelian dealt with static loading capacity of ice and Nguyen et al. with dynamically positioned vessels in level ice.(Su 2011) The large difference in the reported values may be due to the dynamics of icebreaking so that larger relative velocities correspond to higher values of C_f.

Su et al. set C_f to be 3.2 in their simulations on the performance of IB Tor Wiking II as it gave the best fit of results to full scale measurements (Su 2011). This value is taken as a starting point in this thesis and values 3.0, 3.2, 3.5 and 3.8 are used in the sensitivity analysis.

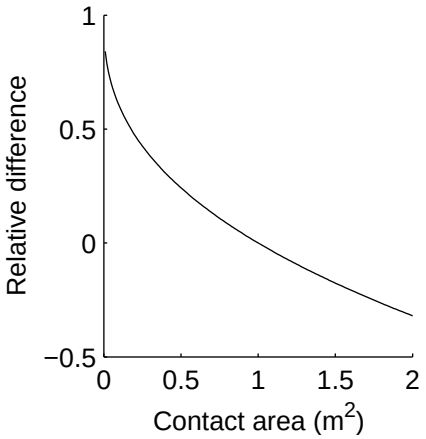

Figure 7: Relative difference of crushing force as a function of nominal contact area calculated using the linear and non-linear crushing model. Positive relative difference indicates that the crushing force according to the non-linear model is larger.

5.2 Alternative crushing models

The two different crushing models produce distinctly different crushing forces for a very wide range of contact areas. As can be seen from figure 7, the non-linear crushing model of equation 19 predicts higher crushing forces than the linear model of equation 21 for nominal contact areas of under 1 m^2 For larger contacts the linear model predicts higher crushing forces. For small contacts the difference is quite pronounced.

The sensitivity analysis outlined in section 5.1 is performed for both crushing models to investigate the overall effect of the crushing model on the motions and loads predicted by the model. Also, the possible effect on the stability of the method is of importance.

6 Comparison of simulated ice loads with full-scale data

The full-scale data that is used to validate the model is described in this section. The measurements were performed during the ARCDEV voyage of MT Uikku in 1998. Loads on selected frames and other phenomena were measured over 12 days of the journey (Kotisalo and Kujala 1998). Measurements to determine the thickness and mechanical properties of ice were also undertaken during the voyage (Hänninen and Lensu 2002).

Table 8: Main particulars of M/T Uikku used for the modeling.(Kotisalo and Kujala 1998)

Length of waterline	156 m
Breadth at waterline	21.5 m
Draught	9.5 m
Volumetric block coefficient	0.68
Waterline opening angle	33°
Flare angle at bow	27°
Hull normal angle at bow	43°
Mass of displacement	22258 t
Mass moment of inertia about the z-axis	3.5×10^9 kgm^2
Bollard pull	1.4 MN
Open water speed	7 m/s

6.1 MT Uikku

Uikku is an ice breaking tanker built in 1977. She has been updated in 1993 and 1998 to make her more suitable for operations in severe ice conditions. The main particulars of MT Uikku are presented in table 8.

In 1998 MT Uikku took part in a voyage to the Kara sea as a part of ARCDEV project. She had been instrumented using strain gauges to measure loads on transversal frames at the bow, bow shoulder and parallel midship area and on longitudinal frames on the midship area. Also stresses on shell plating and transversal frames were measured at bow, bow shoulder, midship and aftship area at the waterline. The instrumentation was carried out by VTT Manufacturing Technology.(Kotisalo and Kujala 1998)

In this thesis measured time histories of frame loads at bow area are compared to simulated results. Location of the instrumented frame used in comparisons is shown in figure 8.

6.2 Full-scale data

A suitable time interval of the recorded load data is chosen for comparison. Uikku operated independently in level ice only on 8.5.1998 from 21:00 to 24:00. The data is

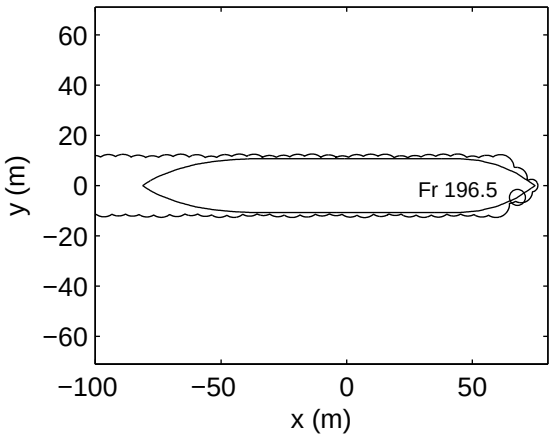

Figure 8: Location of the instrumented bow frame used for comparison with simulated results on the waterline of MT Uikku.

stored in 30 minute files with 600 Hz sampling rate and the selected data are loads on frame 196.5 in the bow area from 22:45 to 23:15. (Hänninen and Lensu 2002)

Test cases of 20 minutes of simulated time were run for the comparison of simulated results with ice loads measured in full scale. The first two minutes of each test case were discarded so that the motions of the ship have settled after encountering the edge of the ice field. An 18 minute segment of the time history was selected for comparison with simulated results. Probability of exceedence plots of different 18 minute intervals selected at random from the data are shown in figure 9. Peak loads were separated from the selected data using Rayleigh separation and loads under 100 kN/m were discarded from the results in the analysis. It can be seen that the shape of the plots is not significantly different in the different cases. The first 18 minutes of the 30 minute variable are selected for comparison with the simulated results.

The details of the ice conditions of the exact time and place of operation of MT Uikku during the examined time period are not known.According to visual observations, the ice thickness was 1.5 m (Kotisalo and Kujala 1998). However, simulations using this ice thickness were not succesfull as all cases resulted in significant sway and yaw motions. A lower ice thickness of 1.35 m was selected. According to Kotisalo and Kujala (1998) the ice thickness after midnight on the night in question was 1.25 m. It can be argued that the value used in the simulations is reasonable given the accuracy of visual observations.

Ice parameters for the simulations were estimated based on the ice thickness and temperature data from observations conducted by the Russian Arctic and Antarctic Research Institute (AARI) on the 5.5.1998 at $71°18'N, 72°08'E$ and 10.8.1998 at $71°48'N, 61°35'E$, near the location where Uikku operated on the 8.5.1998 (Stepanov

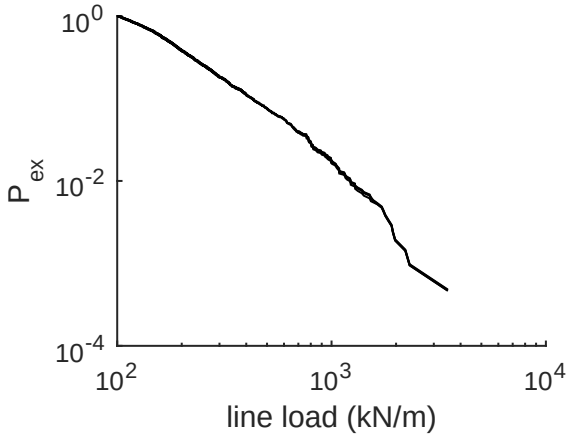

Figure 9: Probability of exceedence plots of four randomly chosen 18 minute intervals of load data from frame 196.5 when MT Uikku is operating independently in thick level ice on 8.5.1998. Differences caused by the selection of analyzed interval on the shape of the plot are negligible.

1998).

The compressive and flexural strength and strain modulus of ice were calculated by the method outlined below. Ice thickness and temperature are needed as input for the method. Here it was assumed that the temperature of ice is the same as air temperature.

The bulk salinity of ice can be estimated based on the ice thickness by a formula by Kovacks (1996a) referenced from (Timco and Weeks 2010)

$$S_i = 4.606 + \frac{91.603}{h_i}, \tag{47}$$

where S_i is salinity of ice in parts per thousand (ppt) and h_i is ice thickness in centimeters. The relative brine volume in ppt can be calculated by as formula by Frankenstein and Garner (1967) referenced from (Timco and Weeks 2010)

$$V_b = S_i \left(\frac{49.185}{|T_i|} + 0.532 \right), \tag{48}$$

where T_i is the temperature of ice in $^\circ C$. The volume fraction of air in the ice can be calculated by

$$V_a = 1 - \frac{\rho}{\rho_i} + \rho S_i \frac{F_2(T_i)}{F_1(T_i)}, \tag{49}$$

where F_1 and F_2 are temperature dependent functions, whose values are given in (Cox and Weeks 1983). The values used in the thesis are given in table 9. ρ is the density of ice in Mg/m^3 and ρ_i is the density of pure ice given by

$$\rho_i = 0.917 - 1.403 T_i \times 10^{-4}. \tag{50}$$

Now, the flexural strength of ice is estimated by a formula by Timco and O'Brien (1994) referenced from (Timco and Weeks 2010)

$$\sigma_f = 1.76 e^{-5.88\sqrt{v_b}}, \tag{51}$$

Table 9: Ice parameters used in the comparison of results with full-scale measurements.

T	-5/-12 °C
F_1	74.662/192.378 Mg/m^3
F_2	0.177/0.240
h_i	1.5 m
σ_c	2.14/4.46 MPa
σ_f	0.45/0.72 MPa
E	5.4/7.7 GPa
μ	0.15
ν	0.3

where v_b is the brine volume fraction and σ_f is in MPa. Further, the compressive strenght of horizontally loaded columnar ice is given by a formula by Kovacks (1996b) referenced from (Timco and Weeks 2010)

$$\sigma_c = 2.7 \times 10^3 \dot{\varepsilon}^{1/3} (v_a + v_b)^{-1}, \tag{52}$$

where $\dot{\varepsilon}$ is the strain rate.

The strain modulus of first-year ice can be calculated by a formula obtained by Timco and Weeks (2010)

$$E = 10 - 0.0351 v_b, \tag{53}$$

where E is the strain modulus in GPa and v_b is the brine volume.

The input parameters and resulting ice properties used for the alculations are given in table 9.

As the choice of the values of the empirical parameters significantly affects the location of ice loads in the simulations, especially for thick ice, a direct comparison of measured and simulated loads of the same frame is not possible. Instead, the simulated loads were converted into line-loads by dividing the crushing forces with the frame spacing for loads shorter than the frame spacing and by the simulated contact length for loads with contact lenght exceeding the frame spacing. Loading time histories of all the frames in the bow area were compiled based on the locations of the loads. Peak loads were separated from the frame time histories, using the same Rayleigh separation algorithm as for the full-scale data and the frame with the highest number of peak loads was selected for comparison in each case.

7 Results

The sensitivity of the model to the empirical parameters C_l, C_v and C_f is presented in subsection 7.1 and the effect of the thickness of ice is examined in subsection 7.2. Results of the comparison of full scale data with simulated results are presented in section 7.3. Breaking pattern, maximum speed in given ice conditions, ice resistance and ice loads are examined in the sensitivity analysis. Only ice loads are examined in the comparison with full-scale data.

Tests for the sensitivity analysis are 600 s of simulated time of the vessel hitting a perpendicular ice edge and penetrating into a homogenous level ice sheet with zero rudder angle. Ice thickness is 0.4 m. Tests that are used for comparison with full-scale data have similar initial conditions but are 1200 s of simulated time and ice thickness of 1.5 m.

7.1 Sensitivity to empirical parameters

The sensitivity of the breaking pattern,maximum speed in ice and ice resistance as well as ice loads to the empirical parameters C_l, C_v and C_f was tested. The distributions of the ice breaking radii normalized by the characteristic length of ice are investigated as there is data available for comparison.

The loads are reported as line loads in order to be consistent with the practice of reporting measured results in full scale. In the case of contact length shorter than the frame spacing the whole load is assumed to be seen by a single frame and the line load is calculated by dividing the contact force with the frame spacing i.e. 0.35 m. This is consistent with the way line loads are determined in full-scale measurements for short contacts acting on single frames. If the contact length is greater than the frame spacing, the line load is calculated by dividing the contact force with the contact length, so as not to exaggerate the line loads. The method for calculating line loads for contact lengths exceeding the frame spacing does not accurately model the measured loads in full scale for such cases, but it is an acceptable simplification given the information available.

7.1.1 Breaking pattern

Figures 10a and 10b show the effect of varying C_v and C_f with constant $C_l = 1$ on the normalized breaking radii for linear and non-linear crushing models respectively. Median values are shown with 5% and 95% quantiles. The shaded area indicates limits of full-scale results presented in table 7.

It is evident from the figures that decreasing the value of C_v causes a decrease in the median value of R/l_c . The value of C_f or the crushing model do not have a significant effect on the breaking radius distributions. The lowest values of C_v give results that best fit the full-scale data in table 7.

Figures 11a and 11b illustrate the influence of varying C_l on the breaking pattern with C_f held constant at 3.8. When the linear crushing model is used, the median value of R/l_c increases with increasing C_l as is to be expected from equation 46. The

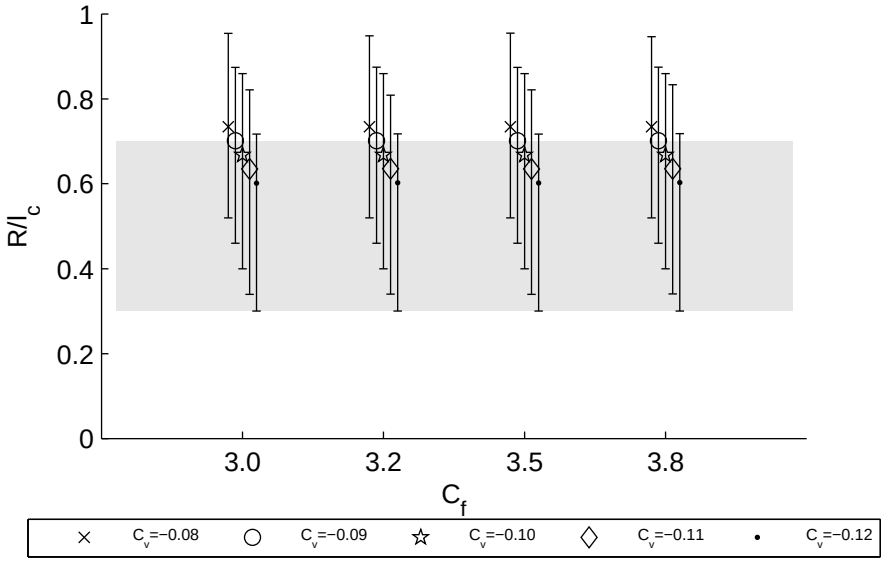

(a) Linear crushing model with $C_l = 1$.

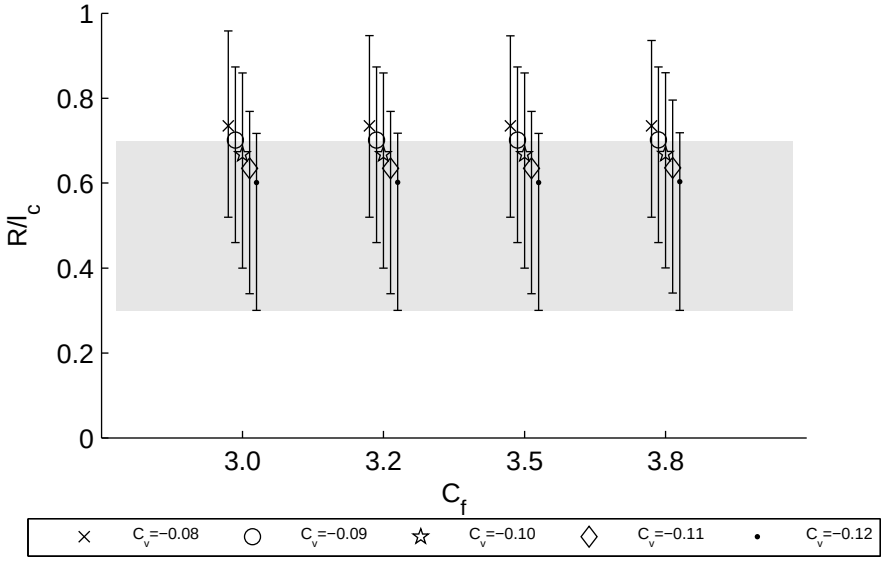

(b) Non-linear crushing model with $C_l = 1$.

Figure 10: Ratio of the radius of broken ice floes to the characteristic length of ice. Shaded area indicates the range of R/l_c for full-scale tests from table 7.

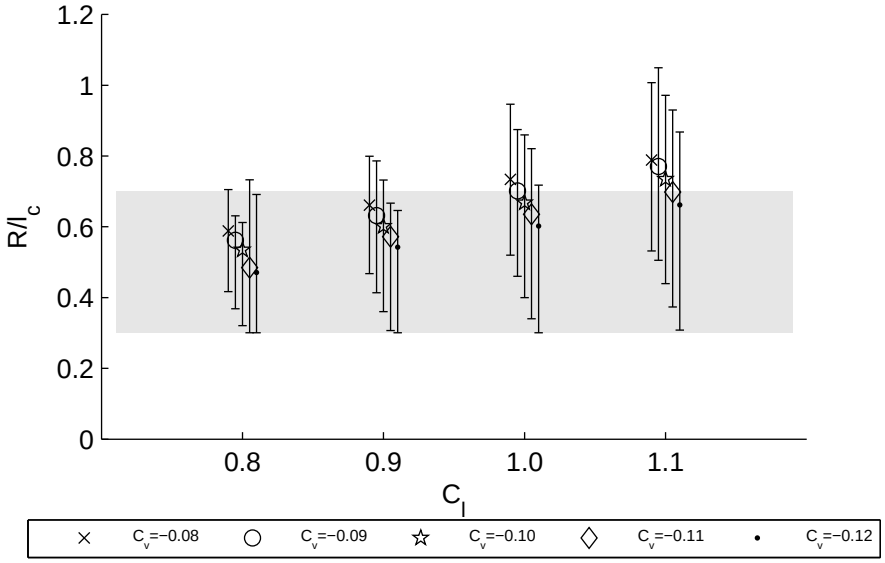

(a) Llinear crushing model with $C_f = 3.8$.

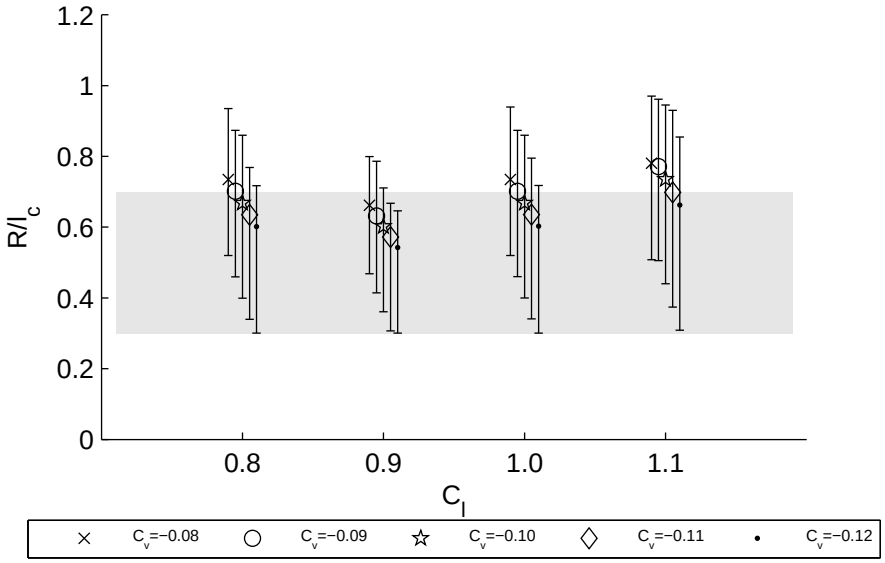

(b) Non-linear crushing model with $C_f = 3.8$.

Figure 11: Ratio of the radius of broken ice floes to the characteristic length of ice. Shaded area indicates the range of R/l_c for full-scale tests from table 7.

range of the results also increases when C_l is increased. With the non-linear crushing model the trend of increasing median of R/l_c with increasing C_l is not as clear as the medians are lower for $C_l = 0.9$ than for $C_l = 0.8$. With both cases values of C_l under 1 produce results that follow the full-scale results from table 7 more closely than the larger values of C_l.

Table 10: Cases with significant sway and yaw motion.

Test parameters				Max deviation	
C_l	C_v	C_f	Crushing model	Y (m)	ψ (degree)
0.8	-0.11	3.8	linear	11	2.5
0.8	-0.12	3.8	linear	9	2.0
1.1	-0.08	3.8	linear	10	2.2
1.1	-0.08	3.8	non-linear	9	2.9

7.1.2 Motions and resistance

In most cases, the choice of parameters did not have a significant effect on the simulated motion of the ship. Surge velocity was very close to 6 m/s except for the combination $C_l = 0.8$, $C_v = -0.11$ and $C_f = 3.8$ with the linear crushing model when the mean surge velocity was about 6.5 m/s. Sway and yaw motion were negligible in most cases. However, in four cases significant sway and yaw motion was evident. These cases are summarized in table 10.

Ice resistance was calculated as the mean of the x-directional component of the forces arising from interaction of ship and ice. The components of ice resistance are crushing and bending resistance and submersion and sliding resistance. The crushing and bending component is the ice resistance is the mean of x-directional ice contact forces from the last minute of simulated time. The submersion and sliding component is the mean value of resistance components calculated using equation 30 over the last minute of simulated time. The submersion and sliding component dominates the overall ice resistance with the relative contribution of contact forces between the ice field and ship ranging from 2 to 8 % of the overall ice resistance.

Calculated resistance values are presented in figures 12a and 12b. When the linear crushing model is used, there is a trend of increasing resistance with decreasing value of C_v and increasing value of C_f. The effect of C_f is more pronounced with lower values of C_v.

The effect of the value of C_f is more pronounced if the non-linear crushing model is used compared to the linear crushing model. The same trends persist as with the linear crushing model and the overall range of predicted resistance is close to the other crushing model.

The small difference in resistances predicted by the different crushing models are expected as the submersion and sliding component of ice resistance, which is not affected by the crushing model, dominates overall ice resistance in all tested cases. In all cases the relative difference of resistances predicted by the different crushing models were within 3 %.

Also C_l has a significant influence in resistance as illustrated in figures 14a and 14b. There is no great difference in the influence of C_l on the resistance with the different crushing models.

Here it should be noted that two cases exhibited irregularities in their time histories of the x-directional forces caused by ice contacts. Time histories of F_{xi} for

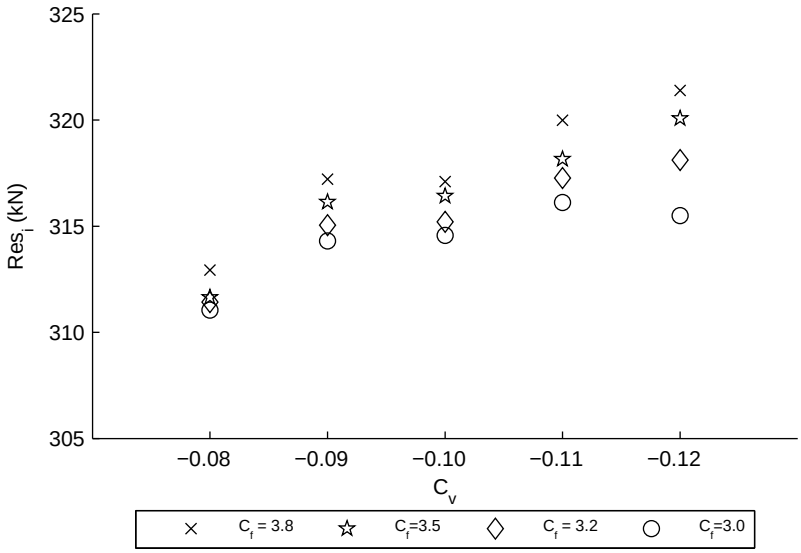

(a) Linear crushing force model.

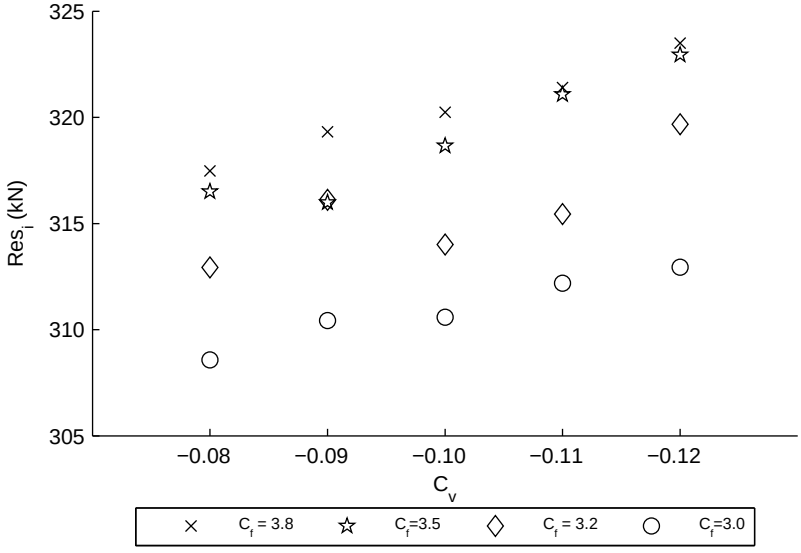

(b) Non-linear crushing force model.

Figure 12: Ice resistance in 0.4 m ice with $C_l = 1$.

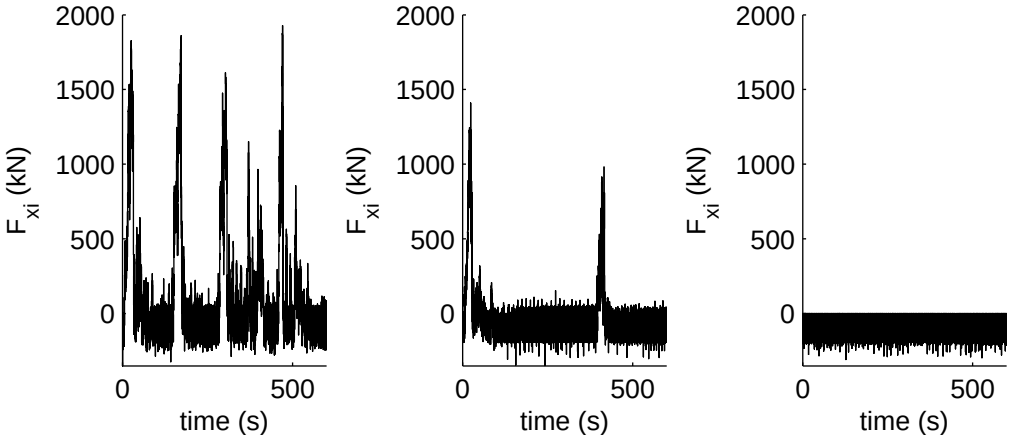

Figure 13: Two anomaly cases of x-directional forces caused by ice contacts and a represantive case of normal behavior (right). In all cases have similar initial conditions and the ship is progressing with zero rudder angle into a homogenous ice field with the initial edge perpendicular to the motion of the ship. $C_f = 3.8$ and the linear crushing model is used in all cases. Other parameters are from left to right $C_l = 0.8$ and $C_v = -0.11$, $C_l = 1.1$ and $C_v = -0.08$, $C_l = 1.0$ and $C_v = -0.09$.

these cases ($C_f = 3.8$, $C_l = 0.8$ and $C_v = -0.11$ as well as $C_f = 3.8$, $C_l = 1.1$ and $C_v = -0.08$, both using the linear crushing model) are shown in figure 13 along a third time history representing a normal case. The positive force peaks in the two leftmost plots in figure 13 are due to ice contacts in the aft shoulder area caused by sway and yaw motion.

This sway and yaw motion is unexpected behavior of the model as the cases are of ships penetrating perpendicularily into a homogenous ice-field with zero rudder. In all cases, except for the four summarized in table 10, the sway and yaw motions were negligible, as was expected as the loads should be symmetric save for numerical inaccuracy and small differences in the discretisation of broken ice edge. However, only two of the four cases with significant sway and yaw motion led to ice contacts in the stern shoulder area.

7.1.3 Ice loads and contact lengths

Loads occuring in the bow area during the last 300 s of simulated time were analyzed. The bow area is defined as the area from the bow to the start of the parallel midship. The calculated loads are separated into load events defined as the effect of a single ice contact. Ice contacts start when the hull and ice edge polygons overlap and stop when the overlap ends due to the relative motion of ship and ice or bending failure of ice. Time histories were analyzed for peak loads using Rayleigh's criterion.

Maximum line loads in the bow area after 300 s of simulated time, with C_l set constant at 1, are shown in figures 15a and 15b. No clear trends corresponding to varying values of C_f or C_v emerge. It is evident, that the different crushing models result in significantly different predictions of line loads. Apart from a single case ($C_l = 1$, $C_v = -0.08$ and $C_f = 3.8$) the line loads predicted by the non-linear crushing

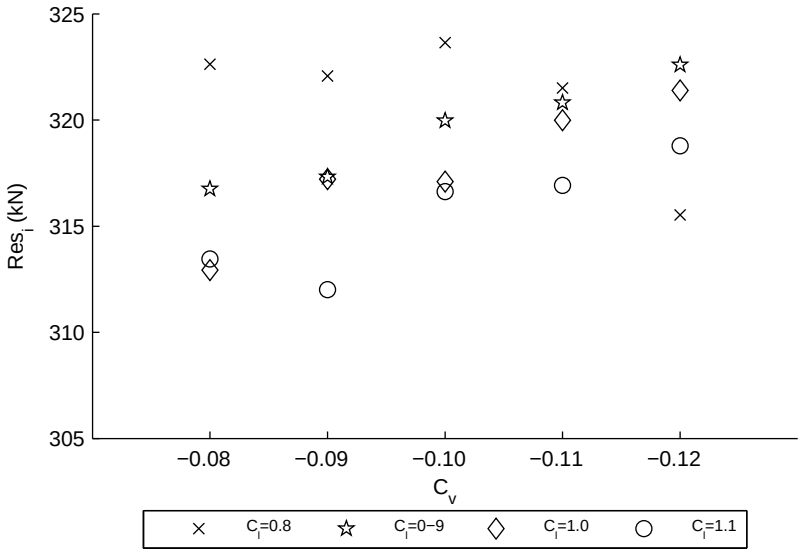

(a) Linear crushing force model.

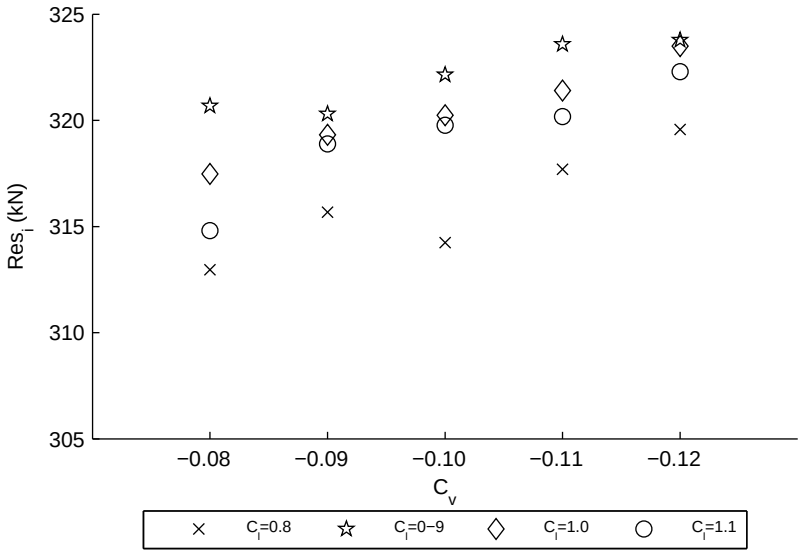

(b) Non-linear crushing force model.

Figure 14: Ice resistance in 0.4 m ice with $C_f = 3.8$.

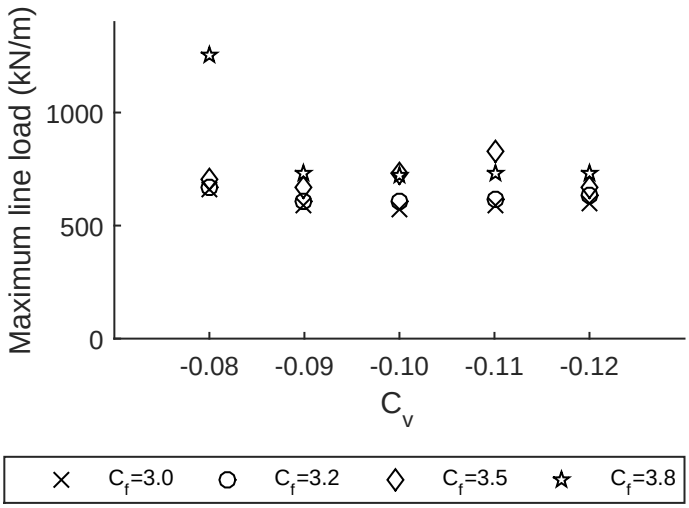

(a) Linear crushing force model.

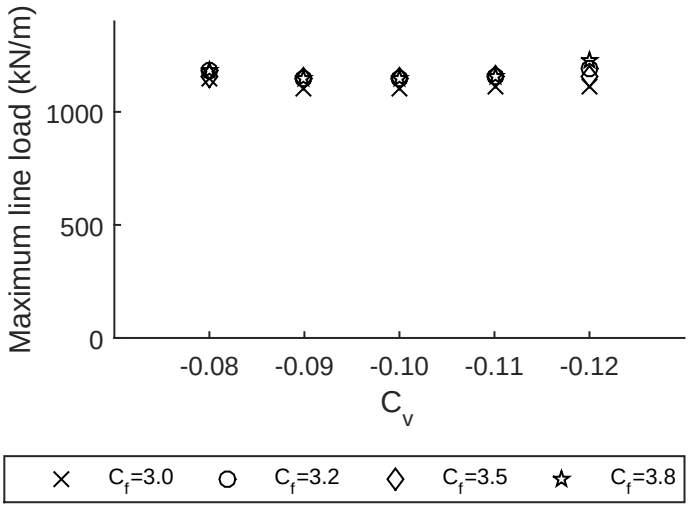

(b) Non-linear crushing force model.

Figure 15: Maximum loads in the bow area, $C_l = 1$.

model are 50-90 % higher than those predicted by the linear crushing model.

Maximum line loads in the bow area after 300 s of simulated time from cases with constant $C_f = 3.8$ are shown in figure 16a and 16b. With the linear crushing model cases with $C_l = 0.8$ produce significantly larger maximum line load predictions than the overall level. Only the case with $C_l = 0.9$ and $C_v = -0.08$ is in line with these results. Rest of the cases predict markedly lower maximum line loads. In the case

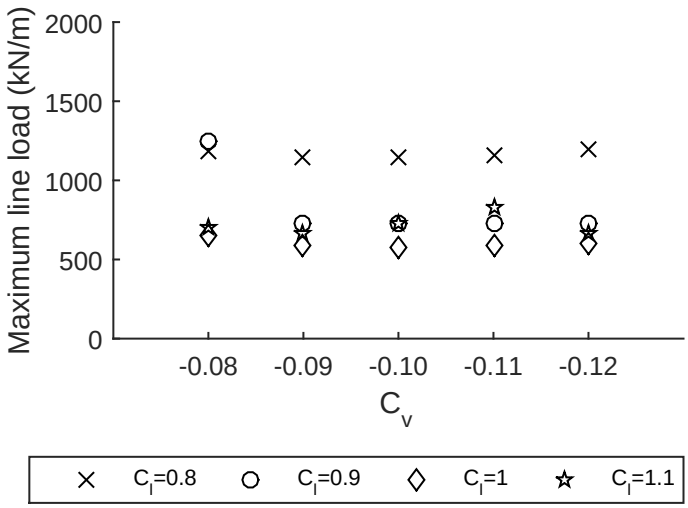

(a) Linear crushing force model.

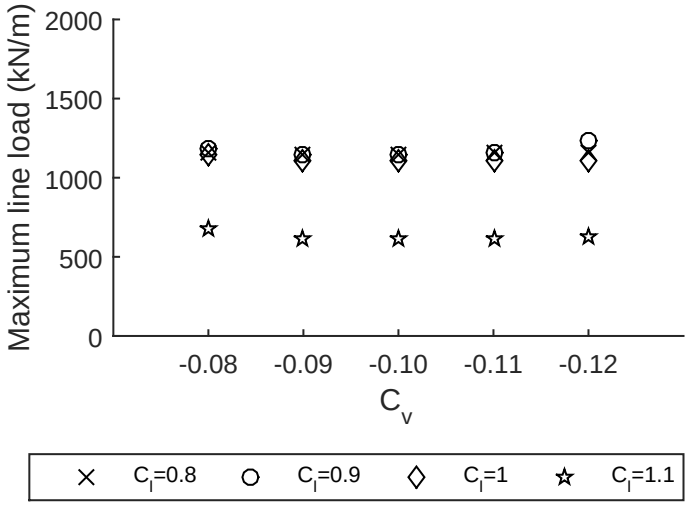

(b) Non-linear crushing force model.

Figure 16: Maximum loads in the bow area, $C_f = 3.8$.

of the non-linear crushing model the cases with $C_l = 1.1$ produce results that are significantly lower than the overall level.

The distributions of contact lengths, defined as the distance between the first and last ice node in a contact, are very skewed and the vast majority of contact lengths is under 1 m, as can be seen from figure 17, where two example cases are shown. The examples give a good impression on the overall shape of the distributions.

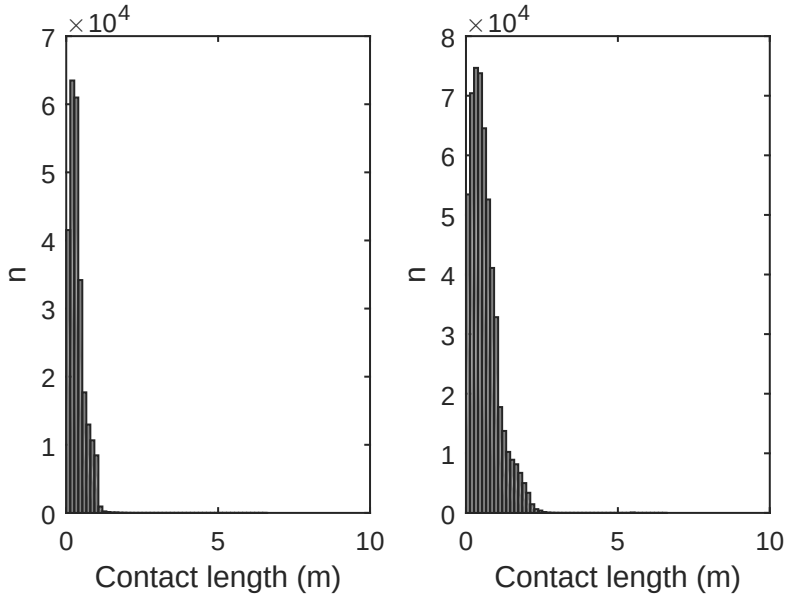

Figure 17: Histograms of simulated lengths of contacts.

The effect of varying C_f and C_v on the simulated contact lengths is illustrated in figures 18a and 18b. Median values as well as 5 % and 95 % quantiles are shown. The non-linear crushing model leads to lower predicted median values of contact length than the linear crushing model. In all cases there is a decreasing trend of the median values with decreasing value of C_v, that is more pronounced with the linear crushing model. With the linear crushing model $C_v = -0.08$ leads to much higher scatter of contact lengths than in other cases.

The higher line loads predicted by the non-linear crushing model with $C_l = 1.0$ can be explained by the lower contact lengths as the calculated maximum crushing forces are roughly similar for both crushing models.

The effect of varying C_f and C_v on the simulated contact lengths is illustrated in figures 19a and 19b. Median values as well as 5 % and 95 % quantiles are shown. Non-linear crushing model leads again to somewhat shorter contact lengths. The cases with $C_l = 1.0$ calculated by the non-linear crushing model exhibit markedly low scatter.

No clear trends emerge in relation to varying values of C_l or C_f for either crushing model. There is a trend of decreasing contact lengths with decreasing value of C_v and the non-linear crushing model leads to shorter contact lengths for constant C_l.

7.2 Effect of ice thickness

Effect of the thickness of ice on the breaking pattern, attainable speed and ice loads was investigated by varying the thickness of ice, while keeping other parameters constant. This was done for several combinations of the empirical parameters. The parameter values used in the calculations are presented in table 11. The values of

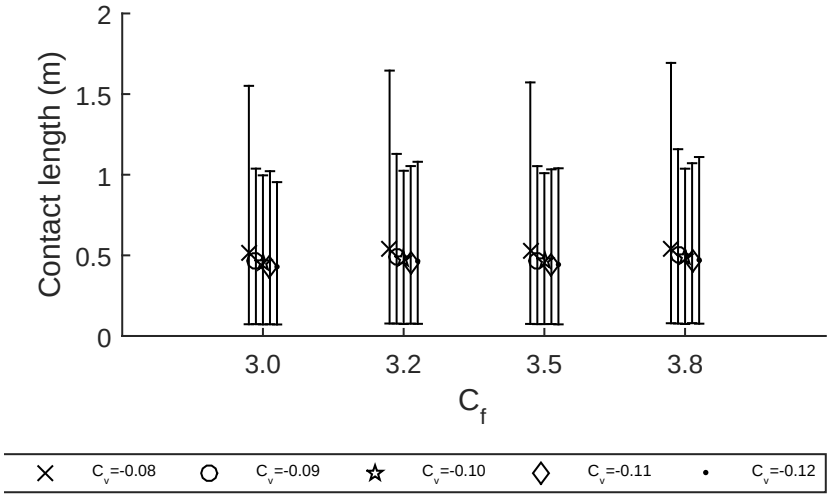

(a) Linear crushing force model.

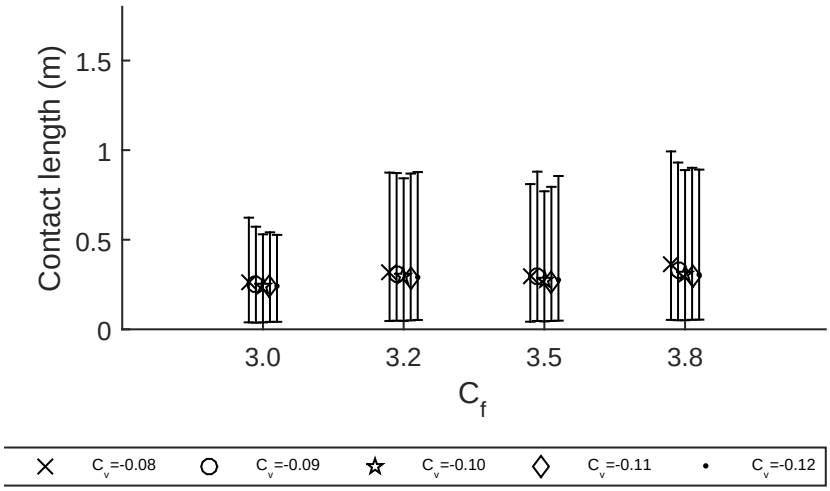

(b) Non-linear crushing force model.

Figure 18: Contact lengths, $C_l = 1.0$. Median values with 5 % and 95 % quantiles are shown.

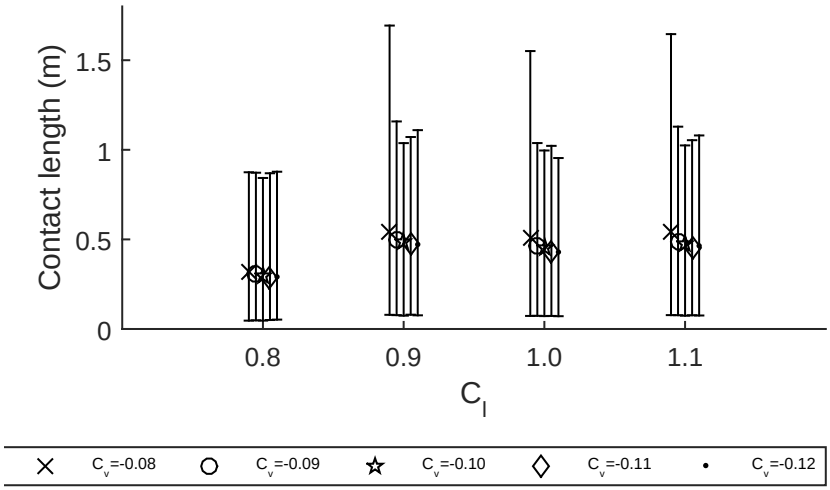

(a) Linear crushing force model.

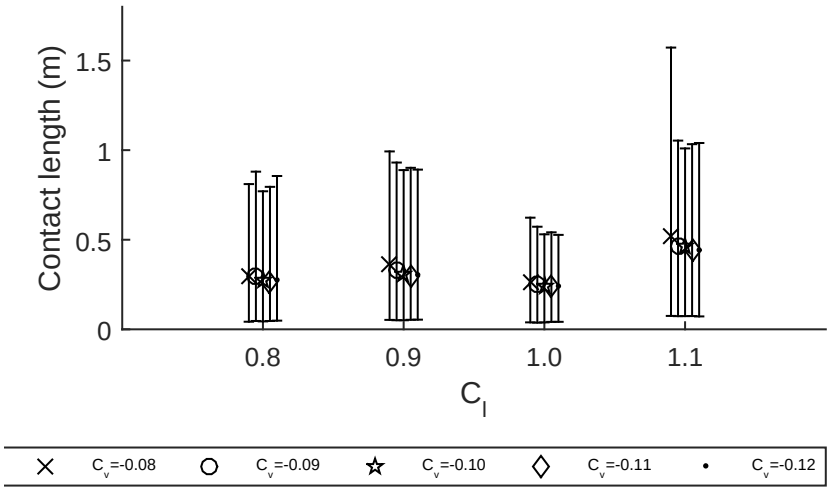

(b) Non-linear crushing force model.

Figure 19: Contact lengths, $C_f = 3.8$. Median values with 5 % and 95 % quantiles are shown.

Table 11: Parameters used in the calculations to determine the effect of ice thickness to the results

h_i	$0.4, 0.6, 0.8, 1.0$ m
σ_c	2.3 MPa
σ_f	0.58 MPa
μ	0.15
C_l	0.8, 1.0
C_v	-0.08, -0.12
C_f	3, 3.8

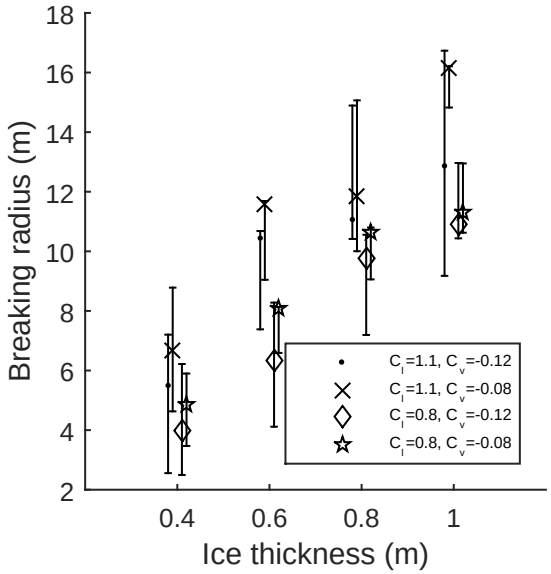

Figure 20: Median values with 5 % and 95 % quantiles of the breaking radii as function of empirical parameters C_l and C_v and ice thickness. C_f is constant at 3.8.

the empirical parameters were chosen to be the extreme ends of the examined ranges of the parameter values in an effort to show the maximum variation of the results.

Median values and 5 % and 95 % quantiles of the breaking radii as function of ice thickness and empirical parameters C_l and C_v are shown in figure 20. It can be seen that the value of C_l has a significant impact on the size of the broken ice floes and that decreasing speed dependence of the breaking radius results in somewhat longer breaking radii. There is an overall trend of increasing breaking radius with increasing ice thickness, which is due to the increase in the characteristic length of ice as per equation 27.

Attainable speeds in different level ice thicknesses were calculated. Simulations were run for 600 s of simulated time and the mean surge velocity during the last 200 s, when the speed has leveled out was calculated for each case and used as the attainable velocity. The velocities calculated for different combinations of the empirical parameters are shown in figure 21 with hv-curves calculated by using the

Table 12: Summary of the cases with unexpected behavior with increasing ice thickness.

C_l	C_v	C_f	
1.1	-0.08	3.0	Decrease of speed with increasing h_i non-monotonic
1.1	-0.08	3.8	Decrease of speed with increasing h_i non-monotonic
1.1	-0.12	3.8	Increase of maximum load with increasing h_i is non-monotonic
0.8	-0.12	3.8	Increase of maximum load with increasing h_i is non-monotonic
0.8	-0.08	3.0	Increase of maximum load with increasing h_i is non-monotonic

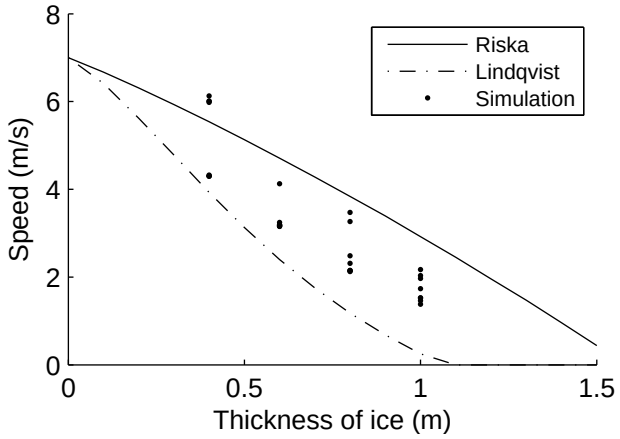

Figure 21: Simulated attainable speeds in different ice thickness plotted with hv-curves calculated using empirical resistance formulas by Lindqvist (1989) and Riska et al. (1997).

empirical resistance prediction formulas by Lindqvist (1989) and Riska et al. (1997) and the net thrust model given by equation 45. Generally, the speeds predicted by the simulation method lie between those given by the empirical formulas, except for some cases with ice thickness of 0.4 m, when the speed predicted by the simulations is higher than given by either empirical method.The empirical formulas differ also significantly in their speed predictions.

The results show an overall trend of decreasing speed with increasing ice thickness with considerable scatter arising from the choice of the values of the empirical parameters. In two cases the predicted speed did not monotonously decrease with increasing ice thickness. These cases are summarized in table 12.

It is also worth noting, that some of the speeds for ice thickness of 0.4 m are considerably slower than those predicted in the cases selected for the sensitivity analysis. The values of the empirical parameters for these cases were the combinations of C_l=0.8 or 1.1 and C_v=-0.12 and -0.08 with C_f=3.0.

The ice resistance varied also in relation to the ice thickness. However the scatter due to the choice of the parameter values was of the same magnitude as the differences between different ice thicknesses as can be seen from figure 22. Especially, in the case of ice thickness of 0.4 m and 0.6 m the general level of ice resistance is almost the same with higher maximum resistances occuring actually for 0.4 m thick ice. The lowest speeds in 0.4 m ice were also near the highest speeds in 0.6 m thick ice.

Maximum predicted line loads are significantly affected by ice thickness as shown

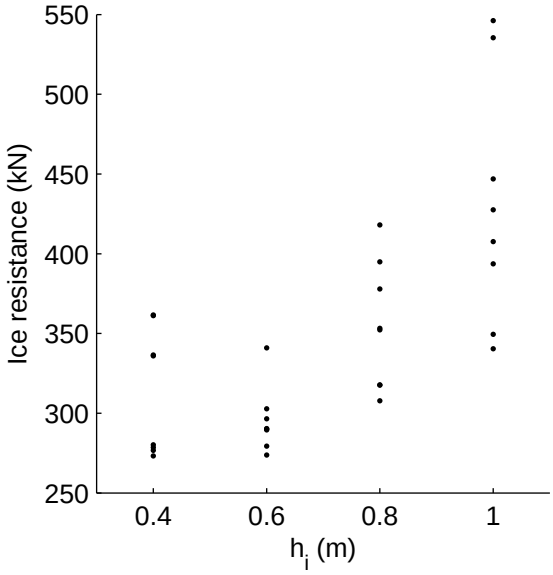

Figure 22: Ice resistance in various ice thicknesses calculated with different combinations of the empirical parameters.

in figure 23. There is an overall trend of increasing maximum load with increasing ice thickness. However, the trend is not monotonic in three cases, which are summarized in table 12. The scatter of the predicted maximum loads within each of the examined ice thicknesses is considerable. The scatter is especially pronounced forice thickness of 1 m.

The large scatter in the results arising due to the choice of the values of the empirical parameters makes it very important to accurately determine the values prior to simulations. It is also important to check the behavior of the simulation model for parameter values given by model tests before commencing the actual simulations.

7.3 Comparison with full-scale data

Simulations were run for 1200 s of simulated time for two ice conditions and the predicted line loads were compared to full-scale data. The empirical parameters could not be kept same for both ice conditions, because of the unstable behavior of the simulation model. No set of the empirical coefficients was fount, that would produce usable results for both ice conditions. For both cases $C_f = 3.5$ and $C_l = 1$. For the case corresponding to ice temperature of -5°C $C_v = -0.10$ and for the other case corresponding to ice temperature of -12°C $C_v = -0.09$.

Two approaches were selected for the comparison with full-scale data. The frame with the most loads was selected for comparison in one approach and the second compared the frame loads from all over the bow area to the measured line loads on a single frame. Not all of the frames in the bow area were loaded in the simulation and each simulated frame experienced considerably fewer peak load events than the

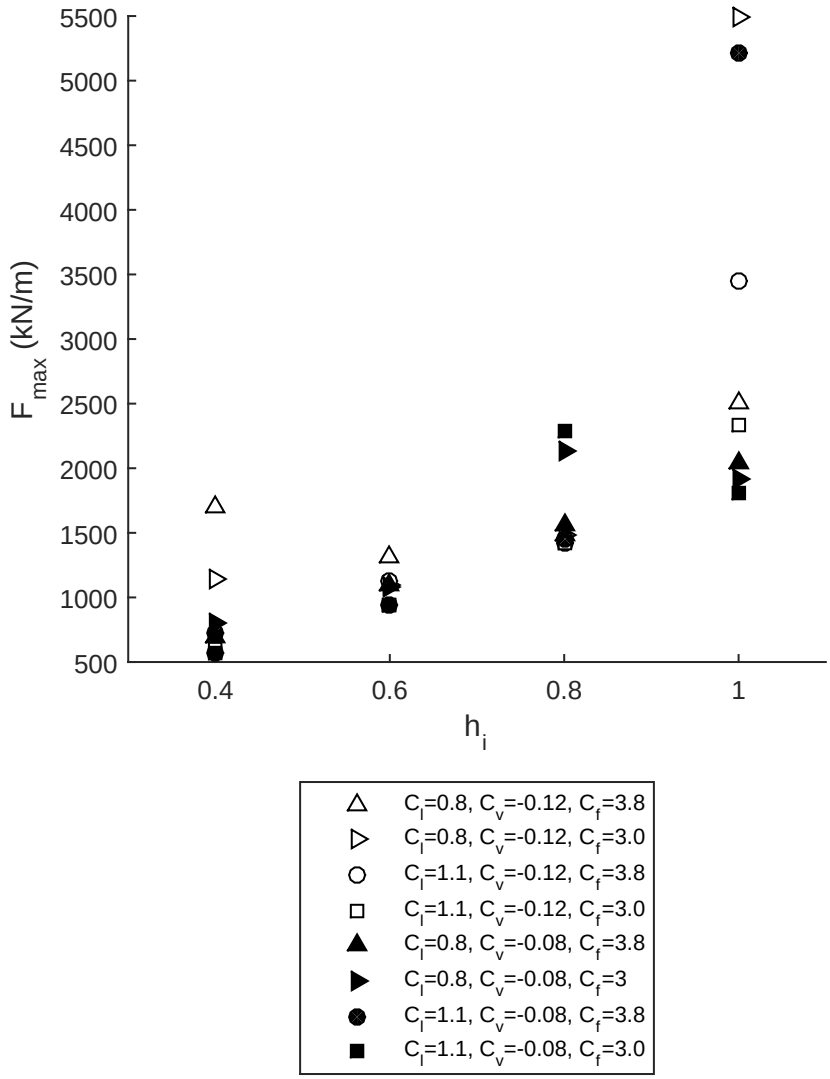

Figure 23: Predicted maximum loads for varying ice thickness with different parameter combinations. Note that the increasing trend is not monotonic for some parameter combinations e.g. $C_f = 0.8$, $C_v = -0.08$ and $C_f = 3$, which predicts higher loads for $h_i = 0.8$ than $h_i = 1.0$.

instrumented frame in the full-scale measurements. For this reason it was not possibe to directly compare the simulated loads on a single frame on the same location as the instrumented frame to the full-scale reasults.

Fgure 24 shows the probability of exceedence plots of the line loads from the two most loaded frames in the simulation results and the full scale data. It can be seen that the low line loads that make up most of the measured data are absent from the simulated results and the total number of loading cases is also lower. This is because no loads on the hull are simulated caused by ice floes that have been broken off the

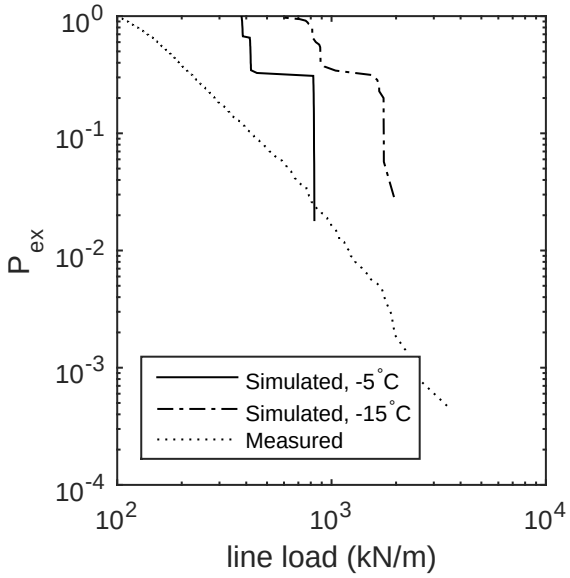

Figure 24: Distributions of the peak line loads from the most loaded frames of the simulated results and the full-scale measurements.

parent ice sheet. At 831 and 1956 kN/mthe maximum line loads are 76% and 43% lower than the measured maximum line load of 3456 kN/m.

The difference in the distribution of the loads is also evident in figure 25, where partial simulated and measured time histories of frame loading are shown. The upper plot is the time period, when loading has occured on the frame with most simulated peak loads in the case corresponding to temperature of -12°C and the lower plot is a measured time history of simiular length. The time interval for the lower plot is chosen to include the maximum measured load in the analyzed time interval.

In the simulated case, the frame loads are clearly grouped in rising saw-tooth patterns, whereas in the measured results the higher loads of over 100 kN/m are more isolated peaks. The absence of small loads in the simulated results is also evident from the time histories. The loading does not seem to occur in similar patterns in the simulated than in the measured data.

Figure 26 shows the probability of exceedence plots of the line loads simulated over the whole bow area and the full-scale data. Again, the small loads are abcent from the simulated results. The shape of the plots is affected by inclusion of more cases and the simulated maximums are higher than for the frames with the maximum number of peak loads. At 2088 and 3899 kN/m the maximum line loads are 40% lower and 11% higher than the measured maximum line load.

The results are summarized in table 13. The results vary significantly based on the selected analysis method. Although selecting the frame with most simulated peak loads for comparison is more in line with the way the full-scale data is recorded, it does not produce very satisfactory results because of the low number of peak loads. The statistical distribution of the peak loads is dissimilar and there is the possibility

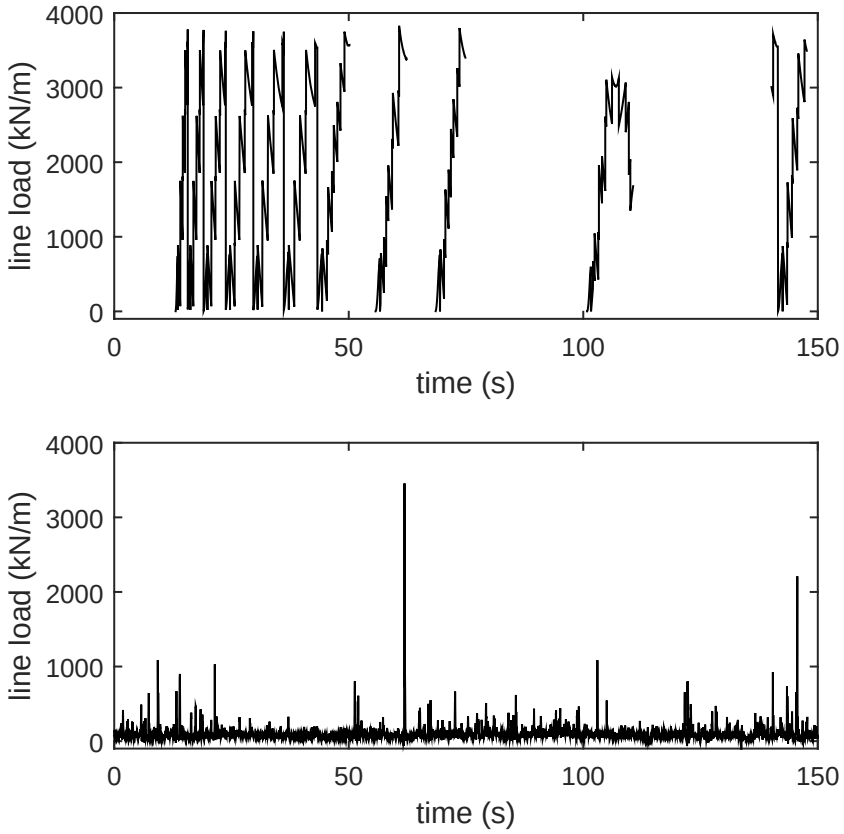

Figure 25: Simulated (top) and measured (bottom) time histories of line loads acting on a frame.

Table 13: Results of the comparison of simulated and full-scale data of line loads.

	Maximum load (kN/m)	Relative difference
Full scale results	3456	
-5°C, most loaded frame	831	-76%
-5°C, whole bow	2088	-40%
-12°C, most loaded frame	1965	-43%
-12°C, whole bow	3829	+11%

of excluding the highest loads as happened in both analysed cases. The most loaded frame is not necessarily the most representative of the loading.

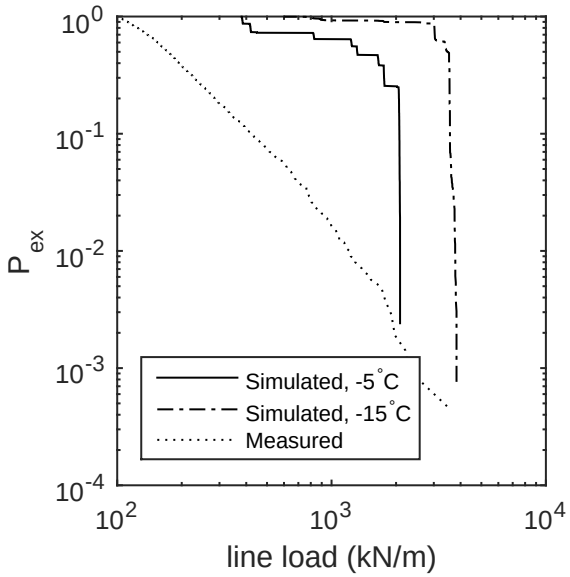

Figure 26: Distributions of the peak line loads from the whole bow area of the simulated results and the full-scale measurements.

8 Discussion on the sensitivity analysis

The sensitivity of the model to the empirical parameters C_v, C_f and C_l was investigated by systematic variation of the parameters. All permutations of $C_f \in \{3.0, 3.2, 3.5, 3.8\}$ and $C_v \in \{-0.12, -0.11, \ldots, -0.08\}$ with $C_l = 1$ were examined using two different crushing force models given by equations 19 and 21. Also all permutations of $C_v \in \{-0.12, -0.11, \ldots, -0.08\}$ and $C_l \in \{0.8, 0.9, 1.0, 1.1\}$ were calculated with $C_f = 3.8$ with both crushing models. The parameter combinations are summarized in table reftestmatrix. Surge velocity, breaking pattern of ice, ice resistance and ice loads were determined in the steady velocity state during the last minute of simulated time. Sway and yaw motion were negligible in most cases but some combinations of parameters were discovered that caused angular motion which affected the locations of ice contacts and resistance calculations.

The range of C_v was determined before the simulations by trying to fit the ice breaking radii associated with the expected range of normal relative velocity of the hull and ice in the contact zones. The value of C_f is difficult to predict a priori as the physical significance of the parameter is not clear. It could reflect the effect of the dynamics of the water foundation in icebreaking. The value chosen by Su (2011) was taken as a starting point in this thesis and variations in both directions were considered. C_l was assumed to be about 1 based on the results summarized in table 7.

Also the effect of ice thickness on the results was investigated by calculating results for selected parameter combinations in ice thickness of 0.4, 0.6, 0.8 and 1.0 m. The absolute breaking radii, resistance, maximum velocity and line loads were examined.

Maximum loads and the distribution of the loads was compared to full scale data in thick level ice. The exact ice conditions during the time of measurement of the full-scale data could not be determined so the simulations were performed for two sets of ice parameters determined based on the ice thickness and available temperature data.

8.1 Breaking pattern

For the sensitivity analysis the breaking pattern was examined by calculating the mean normalied ice breaking radii and their scatter in 0.4 m thick ice. The mean value of R/l_c decreased with increasing absolute value of C_v meaning a stronger speed dependency of the breaking radius. Calculated R/l_c in cases with $C_v = -0.11$ and $C_v = -0.12$ corresponded better to the full-scale results in table 7 than other cases. C_f or the choice of crushing model did not have a significant influence in the breaking radius. The results are summarized in figures 10 and 11 in section 7.1.1.

The effect of ice thickness on the absolute breaking radius of ice was also examined. If C_v and C_l are kept constant, breaking radii grow to over 10 m in ice thickness of over 0.6 m. The fast growth of the breaking radius with increasing ice thickness results in unrealistic breaking patterns especially coupled with the assumption of the shape of the radial crack being circle segments with the center of curvature at the

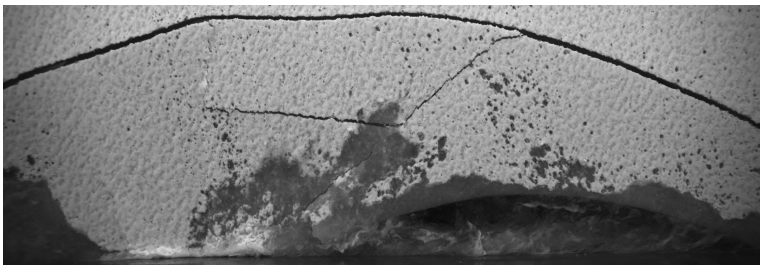

Figure 27: Broken ice floe near the starboard bow shoulder of MS Agulhas II in the Baltic Sea.

midpoint of ship-ice contact. Thick ice results in very few ice contacts compared to thinner ice. Changing ice thickness also influences which part of the bow experiences ice loads.

It would be worth investigating wether C_l and C_v can be assumed to be constant for different ice thicknesses and wether a different assumption should be made concerning the shape of broken ice pieces. Figure 27 shows a broken ice floe near the bow shoulder of MS Agulhas II during the ice trials of the ship. The depth of the floe is significantly less than the width. The shape of the broken floe can not accurately be modeled by a circle segment with the center near the waterline of the ship, suggesting that an alternative model for the breaking pattern could be more accurate.

8.2 Velocity and motions of the ship

The predicted surge velocity is not very sensitive to the varied parameters or the applied crushing model. In the systematic sensitivity analysis where tests were conducted for ice thickness of 0.4 m for parameter combinations shown in table 6 all velocities were within 0.5 m/s at around 6 m/s. However, four additional cases with $h_i = 0.4$ m were calculated to investigate the effect the thickness of ice to the simulation results. These additional cases with $C_l \in \{0.8, 1.1\}$, $C_v \in \{-0.12, -0.08\}$ and $C_f = 3.0$ resulted in significantly lower velocities around 4.3 m/s. It would seem that a more comprehensive sensitivity analysis is called for.

Ice thickness has a strong influence on the speed predicted by the model as can be seen from figure 21 in section 7.2. There is however a large amount of scatter in the speed predictions for given ice thickness depending on the chosen values of the empirical parameters. Furthermore, some parameter combinations did not predict a monotonous decrease in speed with increasing ice thickness.

It would seem, that the method is somewhat uncertain in producing performance predictions in different ice conditions. Several sets of simulations are advisable, so that possible anomalies can be more easily discovered and an idea of the scatter in the predictions can be obtained.

8.3 Ice resistance

Ice resistance is divided into two components in the simulation program. The first component is due to crushing and bending of ice and the second to submersion and sliding of broken ice pieces. The submersion and sliding component, modeled by the empirical resistance formula by Lindqvist (1989), dominates the resistance in 0.4 m thick ice due to the relatively high speeds. Consequently, overall ice resistance is not greatly influenced by the choice of the empirical parameters in thin ice.

There is a trend of growing ice resistance with decreasing value of C_v and increasing value of C_f. The effect of C_l on the ice resistance is less clear. Decreasing C_l increased resistance in 0.4 m thick ice in most cases but not always. The results are summarized in figures 12 and 14 in section 7.1.2

Some tested cases exhibited large positive peaks in the time histories of F_xi, which were due to ship-ice interaction in the aft shoulder area. This behavior of the model is anomalous because in all cases the ship penetrates into a homogenous ice field with zero rudder.

There was considerable scatter in the predicted resistances in different ice thickness. Especially the resistances in ice thickness of 0.4 m and 0.6 m were quite similar. The scatter was more pronounced for thicker ice with the analyzed parameter combinations. Ice resistance is important as such for predicting the powering requierments and energy consumption of ships operating in ice.

The observed scatter in the results and anomalous positive force peaks due to ice contacts in the aft shoulder area mean that care should be taken in analyzing cases for resistance predictions. Several sets of tests are also recommended to be run for similar reasons as given in the end of the previous section.

8.4 Ice loads

The predicted loads were sensitive to the choice of parameters. There were no clear trends associated with varying of the values of the empirical parameters. In the cases with $C_l = 1$ there was one clear outlier when the linear crushing model was used. Apart from this one outlier, the maximum line loads predicted using the non-linear crushing model were significantly higher than those predicted by the linear crushing model. The results are summarized in figure 15 in section 7.1.3.

With constant $C_f = 3.8$, there was one value of C_l that produced a different load level than the overall level of predicted line loads. In the case of the linear crushing model, $C_l = 3.8$ produced significantly higher maximum line loads than the overall level. In the case of the non-linear crushing model, $C_l = 1.1$ produced lower values than the other cases. The results are summarized in figure 16 in section 7.1.3.

Increasing ice thickness tends to increase the predicted maximum ice loads. However, the scatter caused by the selection of the values of the empirical parameters also increases significantly with increasing ice thickness. Also, the number of loading events decreases as ice thickness is increased. The increase of maximum loads with increasing ice thickness is not monotonic for all parameter combinations.

All analysis of the ice loads mentioned above are based on relatively short

Table 14: Summary of the cases exhibiting unexpected behavior. Note that the non-linear crushing model was used only for the sensitivity analysis in 0.4 m ice.

C_l	C_v	C_f	Crushing	Notes
0.8	-0.08	3.0	linear	Outlier surge velocity in 0.4 m ice
0.8	-0.11	3.8	linear	Deviations in sway and yaw, outlier load in 0.4 m ice
0.8	-0.12	3.0	linear	Outlier surge velocity in 0.4 m ice
0.8	-0.12	3.8	linear	Deviations in sway and yaw, outlier load in 0.4 m ice, load increase not monotonic with increasing ice thickness, outlier load in 0.4 m ice
0.9	-0.12	3.5	linear	Outlier load in 1.25 m ice
1.1	-0.08	3.0	linear	Outlier surge velocity in 0.4 m ice, decrease of surge velocity not monotonic with increasing ice thickness, outlier load in 0.4 m ice
1.1	-0.08	3.8	linear	Deviations in sway and yaw, load increase not monotonic with increasing ice thickness
1.1	-0.08	3.8	non-linear	Deviations in sway and yaw, outlier load in 0.4 m ice
1.1	-0.12	3.0	linear	Outlier surge velocity in 0.4 m ice
1.1	-0.12	3.8	linear	Load increase not monotonic with increasing ice thickness

simulations of 5 minutes simulated time. Using longer simulated time intervals might improve results and decrease such behavior of the model that appears erratic when shorter time intervals are analyzed.t

8.5 Summary of the sensitivity of the model

The results of the sensitivity analysis of the ice loads are summarized in table 14. All tests started from similar initial conditions. The method behaves in a stable manner in predicting speeds and resistance in 0.4 m ice for most parameter combinations. However, in thicker ice the scatter is more pronounced and in all tested ice thicknesses outlier cases were found.

Unlike speed and resistance predictions, maximum line loads are sensitive to the crushing model. Both crushing models also show a significant range of load predictions depending on the values of the empirical parameters.

Predicted surge velocities in 0.4 m thick ice were mostly closely spaced. However the parameter values used in the analysis of the effect of ice thickness on the results resulted in significantly lower speeds than most cases. The parameter selection in the analysis of the effect of ice thickness produced significant scatter in speeds in all the tested ice thicknesses.

There appears to be a range of parameters that produce stable, predictable behavior of the model. The irregularities in motion components and loads associated

with cases where $C_l = 0.8$ and $C_l = 1.1$ have to be further analyzed to see wether these are separated incidences or part of a more systematic instability in the model. The analysis conducted in this thesis does not in any way reveal the values of the parameters that produce best results compared to experimental results. It is not possible to say at this point wether the "correct" parameter combinations would be universal or variable case-by-case.

As stated by Su (2011) model tests can be used to set the values for simulation. The use of model tests limits the usability of the model in selecting promising designs for model testing. However if the empirical parameters can be set reliably with the help of model tests the simulation model would be useful in expanding resistance data gained from model tests to further ice conditions and also in load prediction. The sensitivity of the model to mechanical properties of ice would have to be investigated for such work. In cases where model tests are used to determine values for the empirical parameters it would be advisable to perform simulations using parameter values covering the whole range of measurement uncertainty because the predicted results can vary significantly within small ranges of the values of the parameters.

The model is sensitive to the values of the empirical parameters and to the choice of the crushing model. The crushing model affects especially the load predictions. There are not in all cases clear trends in the effect of the parameter values on the predictions produced by the model and some outlier cases are observed. Several sets of simulations should be run to gauge the scatter in the results and identify possible outliers. The method is not as such suitable for producing point estimates of speed, resistance or maximum loads for the aforementioned reasons. However, determining trends based on for example varying ice thickness can help in assessing the reliability of the results.

9 Discussion on the comparison to full-scale data

It is difficult to make a direct comparison of the simulated results and full-scale data for several reasons. The prevalent ice conditions during the measuring of the full-scale data are not known with any accuracy. Visual observations onboard indicate ice thickness of 1.5 m for the night in question that changes to 1.25 m on midnight. Measurement results of ice conditions three days prior and two days after the recording of the full-scale data used in the comparison are available, but these are not from the immediate area of operations of the ship.

The simulation program becomes more unstable in very thick and strong ice, which decreased the amount of simulations it was possible to use for the comparison and the effect of varying empirical parameters could not be estimated. Thick ice causes the program to predict very large breaking radii, which results in a low number of ice contacts in the bow area. A direct comparison of full-scale data from a specific frame and simulated loads acting on the same frame are impossible because some frames may be completely unloaded in the simulations. This problem is exacerbated by thick ice in the simulations. Fourthly, no model tests have been performed to set the empirical parameters for the simulations for this thesis.

However, a set of ice conditions was set based on the available temperature measurements, visual observations of ice thickness and formulations for ice strength and strain modulus based on temperature and ice thickness. The ice thickness indicated in the visual observations could not be used as the simulation method was unstable at such a high ice thickness.

Instead of comparing simulated loads in the same part of the bow as where the measurements were performed, the frames with highers number of peak loads were selected. Also the set of all the peak loads on the bow area was compared to the measured frame loads. The distributions of the measured and simulated loads were clearly different with the measurement data having a significantly higher number of peak loads in the examined time interval than the simulated results. The measured data contains a significantly higher portion of low loads than the simulated results. This can be explained by that the simulation does not model the loads caused by broken ice floes and waves on the frames that are included in the measurement data.

The simulated maximum line loads were mostly in reasonable agreement with the measured maximum load. See table 13 for details. However, the distributions of the line loads were significantly different and the method is not suitable for determining the statistical distribution of loads at least for thick ice. This conclusion is further supported by a comparison of simulated and measured time histories. It would also be advisable to perform several sets of simulations with different parameter because of the scatter evident in the sensitivity analysis.

10 Conclusions and further work

The aims of the thesis set out in section 1.2 were met. Based on the sensitivity analysis, the performance and loads are sensitive to the empirical coefficients. Furthermore, not all of the effects of changing the values of the parameters adhere to any trends. This makes parameter selection important and decreases the usability of the model in predicting loads and performance. Several sets of simulations with varying parameter values are needed to asses the uncertainty in the results, if the model is to be used for predictions.

The effect of ice thickness on the performance and loads was also investigated. For some parameter combinations the effects of increasing ice thickness were not consistent i.e.speed did not decrease of loads increase monotonically with increasing ice thickness. This is a significant problem for the feasibility of the model as a prediction tool. Sets of simulations for different ice thicknesses are also needed to make certain that the selected parameters produce sensible results. Thick ice increases the scatter of predicted maximum loads and decreases the number of ice contacts on the bow area. It would seem that the model is not as such suitable for ice thickness of 1 m or over. It can also be argued, that at this high ice thickness the ice breaking is no longer continuous and heave and pitch motions are relevant to the ice-breaking process and thick ice is outside the scope of the simulation method.

The speeds predicted by the model were compared to two speed predictions using accepted empirical formulas. The speed predictions were overall sensible and were mostly between the predictions of the empirical formulas. There was however significant scatter due to the choice of values of the empirical parameters and no clear advantage over the empirical formulas can be claimed to justify the increase in computational effort.

Two alternative crushing models were investigated and it was found that the predicted maximum loads were significantly affected by the crushing model. The performance prediction was not greatly affected by the crushing model.

Simulated line loads were also compared with full-scale measurements. The predicted maximumloads were mostly in reasonable agreement but the distributions of the loads were significantly different for the simulated and measured results. The model is not suitable to make predictions concerning the statistical distribution of loads but could beused for the prediction of maximum loads if care is taken in the selection of parameters and analysis of the results. Due to the uncertainties in using the model, single simulations should not be used for load predictions.

The sensitivity of the model to ice strength should still be systematically assessed.

The applicability of the model to thick ice could be improved by a new model for the breaking pattern of ice. As illustrated by figure 27 the assumption that the ice floes can be approximated by circle segments centered near the waterline of the ship can be questioned. Especially in thick ice significantly too large ice pieces are cleared by bending failure of the ice sheet and this leads to only few contacts in the bow area.

Stereo camera images from MS Agulhas II or other sources could be used as a basis for a new assumption about the shape of the broken ice floes. Coupled with

data concerning ice thickness obtainable from the images and speed data of Agulhas, a model for the effect of relative velocity and ship speed on the breaking pattern on could also be derived.

Also, detailed investigations in the model tests needed to determine the values of C_l, C_v and C_f is needed to assess the level of uncertainty in the values and to produce good practise methods to obtain reliable estimates of the values. Possible dependency on the ice thickness of C_l and C_v and speed dependency of C_f could also be investigeted with model tests.

References

Berglund, T. (2012). "Ice fracture model for real-time ship simulator". MA thesis. Trondheim: Norvegian University of Science and Technology.

Cox, G. and Weeks, W. (1983). "Equations for determining the gas and brine volumes in sea-ice samples". In: *Journal of Glaciology* 29.102, pp. 306–316.

Daley, C. (2007). "Reanalysis of ice pressure-area relationships". In: *Marine Technology* 44.4, pp. 234–244.

Enkvist, E. (1972). *On the ice resistance encountered by ships operation in the continuous mode of ice breaking.* Report 24. The Swedish Academy of Engineering Sciences in Finland.

Frankenstein, G. and Garner, R. (1967). "Equations for determining the brine volume of sea ice from -0.5 to -22.9 °C". In: *Journal of Glaciology* 6.48, pp. 943–944.

Hänninen, S. and Lensu, M. (2002). *Aspects of Ice Load Monitoring Analysed Using ARCDEV Ice Load Database.* Tech. rep. M-274. Helsinki University of Technology, Ship Laboratory.

Kämäräinen, J. (2007). "Theoretical investigation on the effect of fluid flow between the hull of a ship and ice floes on ice resistance in level ice". PhD thesis. Espoo, Finland: Helsinki University of Technology, Department of Mechanical Engineering, Laboratory for Mechanics of Materials.

Kotisalo, K. and Kujala, P. (1998). *Ice load measurements onboard MT Uikku: Measurement results from the ARCDEV voyage to the Ob estuary, April-May 1998.* Tech. rep. D-47. Espoo, Finland: Helsinki University of Technology, Ship Laboratory.

Kotovirta, V., Jalonen, R., Axell, L., Riska, K., and Berglund, R. (2009). "A System for route optimization in ice-covered waters". In: *Cold Regions Science and Technology* 55, pp. 52–62.

Kovacks, A. (1996a). *Sea ice part 1. Bulk salinity versus ice floe thickness.* Tech. rep. Hanover, NH, USA: CRREL Report 96-7.

— (1996b). *Sea ice part II. Estimating the full-scale tensile, flexural and compressive strength of first-year ice.* Tech. rep. Hanover, NH, USA: CCREL Report 96-11.

Kujala, P. and Riska, K. (2010). *Talvimerenkulku.* Tech. rep. TKK-AM-13. Helsinki University of Technology, Faculty of Engineering and Architechture.

Lau, M., Lawrence, K., and Rothenburg, L. (2006). *Discrete element modeling of ship manouvering in ice.* Tech. rep. Research Council of Canada.

Lensu, M. (2003). *The Evolution of ridged ice fields.* Tech. rep. M-280. Helsinki University of Technology, Ship Laboratory.

Lindqvist, G. (1989). "A straightforward method for calculation of ice resistance of ships". In: *Proceedings 10th International Conference, Port and Ocean Engineering Under Arctic Conditions.* Vol. 2. Luleå, pp. 722–735.

Lubbad, R. and Løset, S. (2011). "A numerical model for real-time simulation of ship ice interaction". In: *Cold Regions Science and technology* 65.2, pp. 111–127.

Matusiak, J. (2013). "Ship Dynamics".

Nevel, D. (1965). *Semi-infinite plate on an elastic foundation.* Research Report 136. Hanover, New Hampshire: U.S. Army Materiel Command, Cold Regions Research & Engineering Laboratory.

— (1968). *The general solution of a wedge on an elastic foundation.* Research Report 247. Hanover, New Hampshire: U.S. Army Materiel Command, Terrestial Sciences Center, Cold Regions Research and Engineering Laboratory.

— (1979). "Bending and Buckling of a wedge on an elastic foundation". In: *Physics and mechanics of ice. IUTAM Symposium.* Copenhagen, Denmark.

Newmark, N. (1959). "A method of computation for structural dynamics". In: *Proceedings of the American Society of Civil Engineers.* Vol. 85. 3, pp. 67–94.

Norman, J. (1980). "Ice resistance prediction and motion simulation for ships operating in the continuous mode of icebreaking". PhD thesis. Ann Arbor, Michigan: The University of Michigan.

Riska, K., Wilhelmson, M., Englund, K., and Leiviskä, T. (1997). *Performance of merchant vessels in ice in the Baltic.* Research Report 52. Helsinki: Winter Navigation Research Board.

Salonen, E.-M. (2003). *Dynamiikka 1.* 9th Edition. Espoo, Otatieto.

Sawamura, J., Riska, K., and Moan, T. (2009). "Numerical simulation of breaking patterns in level ice at ship's bow". In: *Proceedings of the Nineteenth International Offshore and Polar Engineering Conference.* Osaka, Japan, pp. 600–607.

Stepanov, I. (1998). "Ice property measurements during ARCDEV expedition". Unpublished.

Su, B. (2011). "Numerical predictions of of global and local ice loads on ships". PhD thesis. Trondheim: Norwegian University of Science and Technology.

Tan, X., Su, B., Riska, K., and Moan, T. (2013). "A six-degrees-of-freedom numerical model for level ice-ship interaction". In: *Cold Regions Science and Technology* 92, pp. 1–16.

Timco, G. and O'Brien, S (1994). "Flexural strength equation for sea ice". In: *Cold Regions Science and Technology* 22.3, pp. 285–298.

Timco, G. and Weeks, W. (2010). "A rewiew of the engineering properties of sea ice". In: *Cold Regions Science and Technology* 60, pp. 170–129.

Trafi (2014). *Tavaraliikenne.* URL: `http://portal.liikennevirasto.fi/sivu/www/f/liikenneverkko/liikennejarjestelma/tavaraliikenne`.

Vainio, J. and Lumiaro, R. (2013). *Jäätalven ankaruus.* URL: `http://www.itameriportaali.fi/fi/tietoa/yleiskuvaus/jaa/fi_FI/jaatalven_ankaruus/`.

— (2014). *Jäätalvi.* URL: `http://www.itameriportaali.fi/fi/tietoa/yleiskuvaus/jaa/fi_FI/jaatalvi/`.

Valanto, P. (2001). "The Resistance of Ships in Level Ice". In: *SNAME Transactions.* Vol. 109, pp. 53–83.

Wang, S. (2001). "A dynamic model for breaking pattern of level ice by conical structures". PhD thesis. Espoo: Helsinki University of Technology.

Weeks, W. (2010). *On sea ice.* Fairbanks, Alaska, University of Alaska Press.

Yamaguchi, H., Suzuki, Y., Uemura, O., Kato, H., and Izumiyama, K. (1997). "Influence of bow shape on icebreaking resistance in low speed range". In:

Proceedings of the International Conference on Offshore Mechanics and Arctic Engineering, pp. 51–61.

Zhou, L. (2012). "Numerical and experimental investigation of stationkeeping in level ice". PhD thesis. Trondheim: Norvegian University of Science and Technology.